Molecular Clouds in Nearby Galaxies

Yasuo Fukui and Akiko Kawamura

Department of Physics, Nagoya University, Chikusa, Nagoya 464-8602, Japan; email: fukui@a.phys.nagoya-u.ac.jp, kawamura@a.phys.nagoya-u.ac.jp

Annu. Rev. Astro. Astro. 2010. 48:547–80

First published online as a Review in Advance on May 25, 2010

The *Annual Review of Astronomy and Astrophysics* is online at astro.annualreviews.org

This article's doi: 10.1146/annurev-astro-081309-130854

0066-4146/10/0922-0547$20.00

Key Words

galaxies: ISM, galaxies: evolution, galaxies: Local Group, galaxies: Magellanic Clouds, star formation

Abstract

We present a review of spatially resolved giant molecular clouds (GMCs) in nearby galaxies, aiming at providing a template of GMC properties, which may be extrapolated to distant galaxies. We focus on the Magellanic system including the Large and Small Magellanic Clouds (LMC, SMC), M33, and a few dwarfs as observed in the $J = 1$–0 ^{12}CO transition at 2.6-mm wavelength. The X factor, a conversion factor of the ^{12}CO intensity to total molecular column density, and the GMC mass distribution, dN/dM, are similar among these galaxies, suggesting that GMCs share similar properties in the Local Group. The GMCs are classified into three types according to their level of star-formation activity and the types are interpreted in terms of evolution in 20–30 Myr rather than as three different generic types. A three-dimensional comparison including the velocity axis has revealed that GMCs in the LMC are associated with HI envelopes. The HI envelopes are probably gravitationally bound and may be infalling to increase the GMC mass via HI-H_2 conversion. Recent submillimeter observations are revealing dense and warm clumps in GMCs, suggesting that the interior of a GMC also follows contraction leading to star formation on a similar timescale. Finally, we present an attempt to place these GMC properties among more distant galaxies and discuss future observational prospects.

1. INTRODUCTION

Molecular clouds are the densest phase of the interstellar medium (ISM), consisting mainly of molecular hydrogen. Observational studies of giant molecular clouds (GMCs) commenced in the 1970s via large-scale surveys of the Galactic plane in the CO ($J = 1–0$) rotational transition at 2.6-mm wavelength (Dame et al. 1987, Solomon et al. 1987, Combes 1991, and references therein). In the meantime, comparisons with signatures of star formation including young stars like OB associations and HII regions in the solar vicinity revealed that GMCs are where star formation of the entire mass range from low- to high-mass stars occurs (Blitz & Thaddeus 1980). One of the typical examples of a GMC is the Orion A cloud, where active formation of both high- and low-mass stars is taking place (Genzel & Stutzki 1989). However, less massive molecular clouds such as the Taurus dark clouds are the formation sites of only low-mass stars (Mizuno et al. 1995). The typical size of a GMC in the Galaxy is 50 pc to several hundred parsecs, and its mass ranges from 10^4 $M_\odot$ to 10^7 $M_\odot$ (Blitz 1993). Stars, the main constituents of the Galaxy (the Milky Way, hereafter MW), are almost exclusively formed in GMCs. It is therefore important to understand the properties of individual Galactic and extragalactic GMCs including size, velocity dispersion, and mass in our efforts to understand evolution of galaxies from the Local Group to the most distant Universe.

Unfortunately, the velocity and spatial crowding in the MW seriously limits our resolved view of GMCs only to the solar vicinity, making it impossible to list all the Galactic GMCs as a complete catalog except for a limited portion toward the outer MW, where crowding is less significant (Heyer, Carpenter & Snell 2001). However, most of the molecular gas in the vast majority of galaxies is not yet resolved spatially, and their detailed physical properties remained obscured for more than three decades. In the late 1980s, extragalactic GMCs were observed at high enough resolution to spatially resolve them, but systematic efforts to derive general properties of GMCs were hampered by small survey areas in a few galaxies made by the Owens Valley Radio Observatory (OVRO) millimeter interferometer (Wilson & Scoville 1990).

The situation has changed since 1999 as a result of the installation of the NANTEN 4-m telescope in the Southern Hemisphere and the completion of the 10-element Berkeley-Illinois-Maryland Association (BIMA) array in the Northern Hemisphere. The former telescope completed a survey for GMCs in the Large and Small Magellanic Clouds (hereafter, LMC and SMC) at 40-pc resolution (2.6-arcmin beam) at a distance of 50–60 kpc, and the latter was able to resolve GMCs in more distant galaxies in the Local Group at 20- to 50-pc resolution (6- to 13-arcsec synthesized beam) at a distance of 850 kpc. Thus was the first complete survey of GMCs conducted for the LMC and SMC but not for the MW. Subsequently, the BIMA array generated a complete distribution of resolved GMCs in M33. In this way, only recently, the surveys in nearby galaxies began to provide a sample of spatially resolved GMCs, and a new area commenced to comparatively study resolved GMCs in galaxies 30 years after the discovery of GMCs in the Galaxy. In this review, we adopt the following description of the degree of spatial resolution by using the term pixel as the resolution element: "Well resolved" refers to more than ten pixels in a GMC where distribution is studied, "just resolved" indicates a few pixels that allow determination of a GMC size, and "unresolved" indicates only one pixel. The two "resolved" cases correspond to spatial resolution of 40–50 pc and unresolved cases generally have spatial resolution of a few hundred parsecs to kiloparsecs. Most recently, large millimeter telescopes, the Nobeyama Radio Observatory (NRO) 45-m, and Institut de Radio Astronomie Millimétrique (IRAM) 30-m are equipped with millimeter-wave array receivers of 9–25 beams and provide resolved GMC samples vigorously.

We note that the ^{12}CO ($J = 1–0$) emission line is a probe most commonly used to trace molecular clouds because of its low excitation energy (~5 K) and low critical density for collisional

excitation (n_{cr} ~1,000 cm^{-3}). The most abundant species H_2 has no appropriate observable transition in the conditions of GMCs. Recent submillimeter studies opened a new window to probe density and temperature, which was not accessible in the fundamental transition only; the ^{12}CO ($J = 4$–3) transition, for instance, has the upper state at 55 K and a critical density of 1×10^5 cm^{-3}. These submillimeter higher-J CO transitions can selectively trace the warmer and denser interior of a GMC than the $J = 1$–0 CO transition and have the potential to reveal physical properties where star formation is taking place. These submillimeter telescopes include the ASTE 10-m, NANTEN2 4-m, and the Atacama Pathfinder Experiment (APEX) 12-m telescopes located at altitudes around 5,000 m in Atacama, Chile, and have enabled researchers to observe the submillimeter transitions in superb observational conditions following pioneering submillimeter observations with the James Clerk Maxwell Telescope (JCMT) 15-m and the Caltech Submillimeter Observatory (CSO) 10-m telescopes from Mauna Kea.

In this review we shall examine observations of resolved GMCs in disks of nearby galaxies including the LMC, the SMC, M33, etc. and then present a most recent overall picture on the basic properties of GMCs and high-mass star formation therein. We note that observable signs of star formation are limited to those of massive O stars even in these nearby galaxies. We also explore the evolution of GMCs, including their formation and dissipation by comparing GMCs with young objects and HI gas in some of the sample galaxies. This review is organized as follows: In Section 2, we present the galaxies discussed in the review. We present physical properties of GMCs in Section 3 and high-mass star formation and evolution of GMCs in Section 4. GMC formation from HI gas is discussed in Section 5. We give a summary and attempt to place the resolved GMC properties among the average properties of galaxies as well as future prospects in Section 6.

2. INDIVIDUAL GALAXIES

The vast improvement of radio astronomy instruments has enabled researchers to observe extensively the molecular gas in nearby galaxies, in particular those in the Local Group, probing the distribution and properties of the individual GMCs. The target galaxies listed in **Table 1** are dwarf and spiral galaxies in the subgroups of the MW and M31 located within 1 Mpc of the Solar System. The GMCs in these galaxies are resolved at a scale better than 50 pc (see Blitz et al. 2007). In this Section, we introduce these galaxies and examine the global distribution of the CO emission.

Table 1 Properties of galaxies

Galaxy	Morphology	Distance (kpc)	M_B (mag)	Z ($Z_\odot$)
LMC	SBm	50	−18.0	0.5
SMC	SBm	60	−16.7	0.2
NGC 6822	dIrr	500	−15.6	0.3
NGC 185	dSph	660	−14.7	0.3
M32	cE2	780	−16.4	1.1
IC 10	dIrr	820	−16.7	0.25
M31	SAb	830	−21.1	1.0
M33	SAcd	840	−18.9	0.5
NGC 205	E5	850	−15.9	0.8

Note: LMC, Large Magellanic Cloud; SMC, Small Magellanic Cloud.

2.1. The Magellanic System

The Magellanic system consists of the LMC and the SMC with the diffuse gas, the Magellanic Bridge and Stream, connecting both Clouds as well as the MW. They are the best studied nearby galaxies at many wavelengths observationally from the ISM to the stars because of their small distance, 50–60 kpc. Theoretical studies, such as numerical simulations of the tidal structure formation and stellar history, have been also carried out (e.g., Fujimoto & Sofue 1976; Murai & Fujimoto 1980; Gardiner & Noguchi 1996; Yoshizawa & Noguchi 2003; Bekki & Chiba 2005; Růžička, Theis & Palouš 2009). Some researchers have speculated that the molecular features are, in part, due to hydrodynamical collision between the LMC and SMC or ram pressure pileup of gas owing to the motion of the LMC through a halo of hot, diffuse gas (e.g., Bekki & Chiba 2005).

2.1.1. The Large Magellanic Cloud. Among the nearby galaxies, the LMC is the best astrophysical laboratory for studies of the life cycle of baryonic matter because its proximity (∼50 kpc; Feast 1999) and its favorable inclination (35°; van der Marel & Cioni 2001) permit studies of the resolved stellar populations and the interstellar clouds. These conditions allow all LMC features to be at approximately the same distance from the Sun, and there is typically only one or two GMCs along a given line of sight. Accordingly, their relative masses and luminosities can be measured fairly accurately. The LMC also offers the knowledge of the interstellar matter and star-formation processes in an environment with spatially varying subsolar metallicity ($Z \sim 0.3$–$0.5\ Z_\odot$; Westerlund 1997). The dust-to-gas mass ratio has real spatial variations and is ∼2–4 times lower than the value for the Solar Neighborhood (Gordon et al. 2003), resulting in substantially higher UV fields than in the solar vicinity (Israel et al. 1986).

The molecular gas in the LMC has been surveyed for decades (Cohen et al. 1988, Israel et al. 1993, Fukui et al. 1999, Mizuno et al. 2001a, Sorai et al. 2001). **Figure 1** shows the molecular clouds detected with the NANTEN second survey at a spatial resolution of ∼40 pc (Fukui et al. 2008) on an optical image of the LMC. The clouds appear to be spatially well separated, and it is possible to identify them individually, except for a region near the eastern edge of the galaxy, the Molecular Ridge south of 30 Doradus. The long string of bright CO emission is likely composed of several clouds (e.g., Kutner et al. 1997, Indebetouw et al. 2008). The sensitivity of this NANTEN survey is able to detect molecular clouds with $M(\mathrm{H_2}) > 10^4\ \mathrm{M_\odot}$, where $M(\mathrm{H_2})$ stands for the total mass of a molecular cloud observed in CO. Fukui et al. (2008) identified 272 molecular clouds and derived the physical properties such as size, line width, and virial mass for the 164 GMCs that have an extent more than the beam size. Assuming the clouds are in virial equilibrium, an X factor is estimated to be $\sim 7 \times 10^{20}\ \mathrm{cm^{-2}\ (K\ km\ s^{-1})^{-1}}$ to convert CO luminosity to $\mathrm{H_2}$ column density. The mass spectrum of the clouds is fitted well by a power law of $N_{\mathrm{cloud}}[>M(\mathrm{H_2})] \propto M^{-0.75}$ above the completeness limit of $5 \times 10^4\ \mathrm{M_\odot}$. The slope of the mass spectrum becomes steeper if fitting is made only for the massive clouds. Recently, higher resolution observations toward these GMCs have been carried out on the Mopra 22-m telescope. These observations started to resolve the GMCs and enable researchers to discuss the structure and properties within the GMCs (Ott et al. 2008, Pineda et al. 2009).

In **Figure 1**, there is neither an excess nor a deficit of CO associated with the stellar bar but the bright HII regions are clearly associated with molecular clouds. Individual clouds are frequently associated with young clusters or HII regions, but not every cloud shows evidence of such high-mass star formation. Using this association and the ages of the stellar clusters, the evolutionary timescale for GMCs can be established (see Section 4; Kawamura et al. 2009). Comparisons of these clouds with HI gas as well as with the high-mass star/cluster formation were made (see Section 5; Fukui et al. 2009, Kawamura et al. 2009, Wong et al. 2009). Another notable feature in

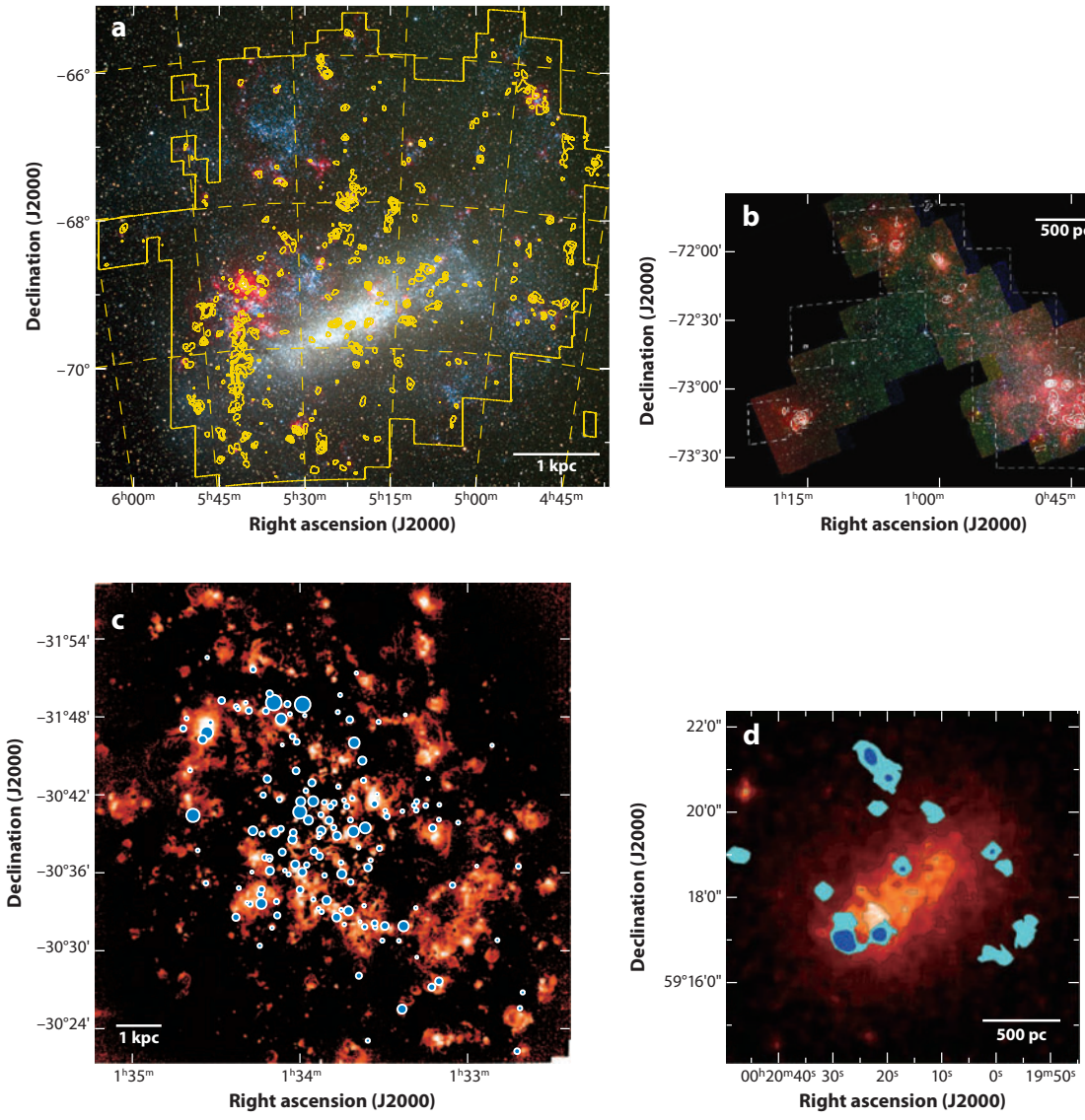

Figure 1

(*a*) Velocity-integrated map of the ^{12}CO emission superposed on an optical image (Fukui et al. 2008). The CO is well correlated with the HII regions. The giant molecular clouds (GMCs) are easily identified by eye except for the region south of 30 Doradus, where they appear as a vertical line of clouds, and the individual GMCs may be overlapping in this region. (*b*) GMCs in the Small Magellanic Cloud observed with the NANTEN telescope (Mizuno et al. 2001b) overlaid on a near-IR image of the galaxy from the *Spitzer Space Telescope* (Bolatto et al. 2007). The lines indicate the survey boundary. The CO clouds are clearly associated with regions of transiently heated small grains or polycyclic aromatic hydrocarbons (PAHs) that appear as bright, nebulous regions on the image. (*c*) The locations of GMCs in M33 as derived from the 759-field Berkeley-Illinois-Maryland Association (BIMA) array mosaic of Engargiola et al. (2003), overlaid on a continuum-subtracted Hα image of the galaxy (Massey et al. 2001). Because the GMCs in a map would be too small to identify in the Figure, the locations of GMCs are instead indicated by blue circles. The area of the circles is scaled to the CO luminosity, which should be proportional to the H_2 mass. (*d*) The GMCs in IC 10, imaged from a 50-field mosaic of the galaxy with the BIMA array, overlaid on a 2-μm image of the galaxy from the 2MASS survey. The light blue area corresponds to CO brightness above 1 K km s^{-1}; the blue area corresponds to CO brightness above 10 K km s^{-1}. The bright region in the center has the highest stellar surface density (Leroy et al. 2006).

the LMC is the existence of the supergiant shells (Meaburn 1980; Book, Chu & Gruendl 2008). These large-scale shells with sizes of more than a few hundred parsecs are often seen in dwarf galaxies and are considered to play an important role in molecular-cloud and star formation. The proximity of the galaxy also enables us to determine the distribution of the interstellar material and star-formation sites to understand the role of these supergiant shells (Oey 1996, Yamaguchi et al. 2001b, Book et al. 2009).

2.1.2. The Small Magellanic Cloud. The SMC is of particular interest because the ISM in dwarf irregular galaxies like the SMC contrasts greatly with that of the grand design galaxies, like the MW, e.g., in their overabundant atomic gas. The SMC, like the LMC, also represents a unique astrophysical laboratory because of its proximity (∼60 kpc; Hilditch, Howarth & Harries 2005), low ISM metallicity (1/5–1/20 $Z_\odot$; Russell & Dopita 1992, Rolleston et al. 1999), and tidally disrupted interaction status (Zaritsky et al. 2004). The SMC offers a rare glimpse into the physical processes in an environment with a metallicity that is below the threshold of 1/4–1/3 $Z_\odot$, where the properties of the ISM in galaxies change significantly as traced by the rapid reduction in the polycyclic aromatic hydrocarbon (PAH) dust mass fractions and dust-to-gas ratios (Draine & Li 2007). The evolution of stars in the SMC is also clearly affected by the low metallicities with the corresponding expected differences in stellar mass loss. These factors should affect the formation and structure of GMCs (e.g., Elmegreen 1989) as well as the star-formation process.

Because of these unique properties, the molecular gas in the SMC has been studied for decades, too. The first attempt to survey the molecular gas in the SMC was done with the Center for Astrophysics 1.2-m telescope by Rubio et al. (1991), covering almost the entire body, 3 deg × 2 deg, at a resolution of ∼160 pc, identifying two molecular complexes in the Bar. Following this survey, high-resolution observations (∼20 pc) with the 15-m Swedish-ESO Submillimeter Telescope (SEST) to indentify molecular clouds and to detect different molecules were carried out (e.g., Rubio, Lequeux & Boulanger 1993; Rubio et al. 1996; Israel et al. 2003c). These observations showed that the molecular clouds detected in CO are mainly distributed in the southern end of the galaxy and are clumpy toward the HII regions.

Figure 1 shows the GMCs superimposed on an IR image of the SMC made using the 3.6-, 4.5-, and 8.0-μm bands from the IRAC instrument on the *Spitzer Space Telescope* (Bolatto et al. 2007). The GMC distribution is from the NANTEN survey at 50-pc resolution and is used to derive an X factor $(14 \pm 3) \times 10^{20}$ cm^{-2} (K km s^{-1})$^{-1}$ (Mizuno et al. 2001b). As in the LMC, the GMCs in the SMC are easily identified individually. However, unlike the LMC, they are not spread throughout the galaxy but appear preferentially on the northern and southern ends of the galaxy. Another grouping is located to the east of the SMC along the HI bridge that connects the LMC and SMC, apparently outside the stellar confines of the galaxy. The *Spitzer* image traces the stellar continuum as well as warm dust and PAH emission. The 8.0-μm emission is associated with the molecular gas traced by CO, but appears to be more extended than the CO emission (see Section 3). These characteristics are also seen for the HII regions; the GMCs show a good spatial correlation with HII regions, but large HII regions are usually more extended than the CO emission. The GMCs also show a good correlation with young clusters (Bica & Schmitt 1995, Bica & Dutra 2000). These facts, together with the results that the GMCs show little association with older clusters and SNRs, suggest the rapid dissipation of molecular clouds traced by CO.

2.1.3. The Magellanic Bridge. The Magellanic Bridge is a part of a filament of neutral hydrogen, which joins the SMC and LMC over ∼20 kpc (Staveley-Smith et al. 1998; Muller, Staveley-Smith & Zealey 2003; Muller et al. 2004). The LMC and the SMC represent the nearest example of tidally interacting galaxies, and the Magellanic Bridge is a clear manifestation of a close encounter

between these two galaxies some 200 Myr ago (Gardiner & Noguchi 1996, Zaritsky et al. 2004). Over cosmological timescales, galaxy interactions are one of the key drivers of galaxy evolution and, thus, tidally interacting galaxies allow researchers to examine star formation in an unusual and disturbed environment, which resembles the conditions in the early Universe. Recent studies have revealed the presence of locally formed, young (<200 Myr) high-mass stars associated with the highest-density portion of the Bridge, which is adjacent to the main SMC body (Harris 2007).

The Magellanic Bridge is characterized by substantially lower metallicity (1/20 $Z_\odot$) than the main SMC body (Rolleston et al. 1993, 1996, 1999), making it a unique laboratory to study star formation in a low-metallicity environment. Young stars in the Bridge have ages as low as ~7 Myr, substantially less than the age of the encounter, indicating in situ star formation. This motivates the search for star-forming molecular gas. After several unsuccessful searches, the first detection of a molecular cloud in the Bridge was made by Muller, Staveley-Smith & Zealey (2003) in the ^{12}CO ($J = 1$–0) transition. Subsequent to the discovery, Mizuno et al. (2006) carried out an exhaustive search for molecular gas down to 3 mK rms for 1.0 km s^{-1} velocity resolution at 40 positions corresponding to a coverage of 200 arcmin^2, toward the major far-IR and HI peaks with the NANTEN telescope and detected seven regions in addition to the cloud of Muller et al. This coverage is more than 30 times larger than those of the other surveys of a few pointings with a few 10-arcsec beams (Muller, Staveley-Smith & Zealey 2003). The cloud masses of these regions are (1–7) $\times 10^3$ $M_\odot$ assuming the X factor of the SMC and the total molecular mass is 2×10^4 $M_\odot$, similar to the Taurus complex, as compared to the HI mass of $\sim 5 \times 10^7$ $M_\odot$ in the Bridge (Putman et al. 1998). Mizuno et al. (2006) estimated the star-formation rate to be $\sim 6 \times 10^{-4}$ $M_\odot$ year^{-1} and suggested that the Bridge may evolve into a third Magellanic Cloud. The Magellanic Stream extending further out has a much lower HI column density than the Bridge and seems too faint to detect CO.

2.2. M33

M33, a spiral in the Local Group, is also one of the galaxies that, owing to its proximity and low inclination, permits direct and detailed comparisons of molecular, atomic, and ionized hydrogen gas on the scale of individual GMCs. Interferometric observations enable researchers to resolve the molecular gas into individual molecular clouds, and the early observations from OVRO showed that GMCs in part of the galaxy have size and mass similar to the MW GMCs (Wilson & Scoville 1990). **Figure 1** shows the locations of GMCs for the entire extent of M33 in observations from the BIMA array at 50-pc resolution (Engargiola et al. 2003, Rosolowsky et al. 2003) superimposed on an Hα image of the galaxy (Massey et al. 2001). From these data, Engargiola et al. (2003) generated a catalog of 148 GMCs with a detection limit to GMC masses of 1.5×10^5 $M_\odot$, where an X factor of 2×10^{20} cm^{-2} (K km s^{-1})$^{-1}$ (Blitz et al. 2007) was used to convert L_{CO} into $M(H_2)$. The two low-contrast spiral arms (Regan & Vogel 1994) are well traced by GMCs, but the GMCs are not confined to these arms, as is evident in the center of the galaxy. There is a good spatial correlation between the GMCs and the HII regions, and more than two-thirds of the GMCs have associated HII regions. As with the LMC, the correlation is not perfect and there are GMCs without HII regions and vice versa. There are presumably many lower mass clouds below the limit of sensitivity. Many of these low-mass clouds are likely associated with the unaccompanied HII regions in **Figure 1**.

The GMCs in the catalog are confined largely to the central region ($R < 4$ kpc). They show a remarkable spatial and kinematic correlation with overdense HI filaments (Engargiola et al. 2003); the geometry suggests that the formation of GMCs follows that of the filaments. The GMCs exhibit a mass spectrum $dN/dM = M^{-2.6\pm0.3}$, which is considerably steeper than that found in the MW and in the LMC. Combined with the total mass estimated by the X factor,

this steep function implies that the GMCs in M33 form with a characteristic mass of $\sim 7 \times 10^4$ $M_\odot$ (Rosolowsky 2005). Follow-up of these surveys at higher sensitivity is ongoing with the NRO 45-m telescope, and these new results generally support the BIMA results (Rosolowsky et al. 2007, Tosaki et al. 2007a).

2.3. M31

The Andromeda Galaxy (M31) is the second largest disk galaxy in the Local Group, after the MW, and has outstanding spiral arms. It subtends over 2 deg $\times$ 0.5 deg in the sky. Its proximity makes it an excellent target for studying extragalactic molecular clouds, although the large inclination angle makes association among objects less certain. Numerous surveys of CO emission have been conducted over portions of M31, and a comprehensive list of the 24 CO studies published up through 1999 is given in Loinard et al. (1999). This extensive list of surveys can be supplemented with a few major studies that have occurred since then.

An extensive survey covering the entirety of the star-forming disk of M31 has been completed using the IRAM 30-m telescope at 85-pc resolution; large-scale arms and inter-arms showing CO intensity contrast of 0.3–0.6 are clearly resolved (Nieten et al. 2006, and references therein). The CO intensity shows a good correlation with the far-IR radiation at 175 μm, indicating that molecular gas is well correlated with high-mass star formation. Nonetheless, resolution somewhat larger than the GMC size seems to have hampered resolving GMCs under the large inclination angle. Subsequently, Sheth et al. (2008) used the BIMA array to study 30 fields in the outer region of the galaxy and found six molecular complexes similar to those found in the inner part of the MW, and Rosolowsky (2007) carried out BIMA observations along a spiral arm. The latter study identified 67 GMCs and derived physical parameters for 19 resolved GMCs. More recently, millimeter and submillimeter observations of giant-molecular-cloud associations (GMAs) were carried out in the southern spiral arm on the NRO 45-m and ASTE 10-m telescopes (Tosaki et al. 2007b). These observations suggest that the molecular gas consists of two velocity components, one of which is the postshock dense gas produced by shocks due to a density wave.

2.4. IC 10

IC 10 is a dwarf irregular galaxy with a huge envelope of HI extending seven times farther than its optical diameter and stretching nearly a degree on the sky (Huchtmeier, Seiradikis & Materne 1981). The metallicity is 1/5 $Z_\odot$ (Garnett 1990), lower than those of the MW and LMC but a little higher than that of the SMC. The integrated optical magnitude and total HI mass are comparable to those of the SMC. However, based on its star-formation rate of ~ 0.15 $M_\odot$ Myr^{-1} (Thronson et al. 1990) and the number of Wolf-Rayet stars (Massey & Armandroff 1995), IC 10 is considered to be a starburst galaxy. The current star-formation activity is concentrated around a large HI cloud in the southeastern region, which contains the most luminous HII regions (Hodge & Lee 1990), nearly half of the Wolf-Rayet stars (Massey & Armandro 1995), and a large nonthermal superbubble indicative of recent supernovae explosions (Yang & Skillman 1993).

The first detection of CO emission was reported by Rowan-Robinson, Phillips & White (1980) with the National Radio Astronomy Observatory (NRAO) 11-m telescope. Observations with the NRO 45-m telescope (Ohta, Sasaki & Saito 1988) showed that the molecular gas consists of a few molecular clouds, which are well associated with star-forming regions and HI gas. Further observations by interferometers (OVRO, Wilson & Reid 1991; Nobeyama Millimeter Array, Ohta et al. 1992; OVRO, Wilson 1995) showed that the size, line width, and mass are consistent with those of the MW, M31, and M33. Bolatto et al. (2000) carried out submillimeter observations of

Table 2 X factor

Galaxy	Mean $X_{CO} \times 10^{20}$ cm^{-2} (K km s^{-1})$^{-1}$	Reference(s)
LMC	7 ± 2	Fukui et al. 2008
SMC	14 ± 3	Mizuno et al. 2001b, Blitz et al. 2007
M31	5.6 ± 1.1	Rosolowsky & Leroy 2006
M33	3.0 ± 0.4	Engargiola et al. 2003
IC10	2.6 ± 0.5	Leroy et al. 2006

the most massive molecular cloud in CI, ^{12}CO ($J = 3$–2), and ^{13}CO ($J = 3$–2) transitions as well as 850-μm and 1,350-μm dust continua on the JCMT. They found that the intensity ratio of [CI] and CO is similar to that in the GMC in the solar vicinity and in the N159 in the LMC despite the low metallicity, suggesting that the origin of the atomic carbon is from the photodissociation.

Figure 1 is an image of the GMCs in IC 10 from a 50-field CO mosaic from the BIMA array (Leroy et al. 2006) superimposed on a 2-μm image (Jarrett et al. 2003). As with the Magellanic Clouds and M33, the GMCs show no obvious spatial correlation with the old stellar population—some massive clouds are found where there are relatively few stars. Leroy et al. (2006) derived an X factor (2.6 ± 0.5) × 10^{20} cm^{-2} (K km s^{-1})$^{-1}$ as listed in **Table 2**. This value is about a factor of two smaller than that previously estimated (Wilson 1995), and Leroy et al (2006) noted that the difference is due to the lower intensity in the previous OVRO data. A simple correlation between an X factor and metallicity is not supported here. Leroy et al. (2006) estimate the total CO luminosity to be 2.2 × 10^6 K km s^{-1} pc^2 by combining NRAO 12-m data and find that the star-formation efficiency is higher than that of large spiral galaxies. There are a few possible explanations for this, one of which is the idea that IC 10 is in the phase just after the peak of a starburst so that the signatures of star formation are still present but the star-forming gas has already been somewhat depleted (Leroy et al. 2006).

2.5. Dwarfs

The Local Group dwarf galaxies offer a unique laboratory to study the detailed properties of most common types of galaxy in the Universe (e.g., Mateo 1998). Evidence for interstellar dust clouds has been observed optically in some dwarf irregular galaxies and near the cores of some dwarf spheroidals. Most of the dwarf irregular galaxies host fairly large HII regions, such as Hubble V in NGC 6822. There have been a few attempts to detect CO emission from these galaxies, and more than 10 dwarf irregular galaxies in the Local Group are found to host molecular gas detected in CO (e.g., Israel 1997). Nonetheless, the weak emission from the molecular gas makes it hard to survey molecular clouds in these galaxies, such that many of the observations are pointed toward these HII regions. The examples of the observations are by SEST, JCMT, IRAM, and NRO, with a relatively large aperture.

NGC 6822 is one of the Local Group dwarf irregular galaxies at a distance of 500 kpc (McAlary et al. 1983) from which the detection of molecular gas has been tried since the early 1980s (Elmegreen, Morris & Elmegreen 1980; Wilson 1992; Israel et al. 1993; Ohta et al. 1993). The metal abundance of its HII regions is relatively low ([O/H] = 1.7 × 10^{-4}) (Skillman, Terlevich & Melnick 1989) and about one-third that of the Solar Neighborhood and between those given by Dufour (1984) for the LMC and the SMC. Major OB associations, as well as the large, bright HII regions Hubble I, III, V, and X (Hubble 1925), are found at the northern end of the bar. Despite its large number of HII regions, NGC 6822 is not very active in forming stars (e.g., Gallagher et al. 1991).

Until recently, CO emission has been detected from several positions toward the HII region complexes including Hubble V (Wilson 1992, 1995; Ohta et al. 1993). Recently, CO ($J = 2$–1) mapping using the HERA on the 30-m IRAM telescope was carried out, and the largest sample of 15 GMCs was obtained (Gratier et al. 2010). There is no clear difference between the properties of the GMCs in NGC 6822 and those of the MW except lower CO luminosities for a given mass, despite the much lower metallicity. The total H_2 mass is estimated to be less than 10^7 $M_\odot$. This corresponds to an X factor of about 4×10^{21} cm^{-2} (K km s^{-1})$^{-1}$ (Gratier et al. 2010).

Some attempts to detect molecular gas toward the nearest dwarf elliptical galaxies are also being carried out. Young (2001) observed NGC 185 and NGC 205 with the BIMA in the M31 group. The molecular gas is mostly detected in one resolved cloud, and the size, velocity width, and so on are found to be similar to those in the larger galaxies (Young 2001).

2.6. Searches for Molecular Gas in Distant Galaxies

Studies of the molecular gas in more distant nearby galaxies have been carried out over the decade with a few approaches. Earlier studies in the 1980s are examined in Young & Scoville (1991), who summarize detailed analyses of the nearby galaxies and the global properties of selected samples. The former needs high-resolution observations, and the early studies were limited to a few 100 pc for the LMC and about a kiloparsec for the others. Nevertheless, the role of molecular gas in spiral structure and star burst galactic nuclei as well as properties of some GMAs in the Local Group galaxies were provided. These studies on 400 galaxies revealed the following main properties of large-scale molecular distribution (Young & Scoville 1991):

1) Total molecular mass in a galaxy ranges from less than 10^6 $M_\odot$ to 5×10^{10} $M_\odot$ with a kiloparsec-scale surface mass density in the disk from 1 to 30 $M_\odot$ pc^{-2}.
2) The molecular to atomic mass ratio ranges from 4 to 0.2, following the Hubble type from S0/Sa to Sd/Sm.
3) Radial distribution of molecular gas is more centrally concentrated globally than HI, and the spiral structure is traced by molecular gas locally.
4) Molecular gas is star forming and becomes bright in the infrared by stellar energy release. The infrared luminosity-to-mass ratio, $L_{IR}/M(H_2)$, is fairly constant at around 10 $L_\odot$ $M_\odot{}^{-1}$. The ratio Hα/CO is also enhanced in the arm, where star formation is active, relative to the inter arm.

The improvement of the instrumental capabilities advanced the molecular gas studies of the nearby galaxies both in detail and globally since the 1980s. There have been a number of surveys with the resolution high enough to study the properties of the molecular gas and star formation with a resolution of about a few kiloparsecs or higher. Individual galaxies like M51 (e.g., Schuster et al. 2007, Koda et al. 2009), NGC 253 (e.g., Sakamoto et al. 2006), and M83 (e.g., Crosthwaite et al. 2002) have been intensively observed along with statistical studies for galaxy samples (e.g., Helfer et al. 2003; Kuno et al. 2007, 2008; Leroy et al. 2009b), leading to the enhanced star formation related to galactic bars and spiral arms.

The direct detection of molecular gas in dwarf irregular galaxies and/or those of low metallicity beyond the Local Group also has been carried out extensively. These galaxies are thought to be difficult to observe in molecular emission, but their environments provide us with some knowledge of the properties of the ISM in the early Universe. Observations have been done especially toward active star-forming regions, e.g., NGC 1569 (Kobulnicky & Skillman 1997), and show that the cloud properties are compatible with the GMCs in the MW (Bolatto et al. 2008). It is also found that the CO luminosity is correlated well with the K-band luminosities and high-mass star-formation

rate, though there is no strong dependence of the X factor to metallicity in the range of $0.25\ Z_\odot < Z < 1\ Z_\odot$ (Leroy et al. 2009b).

Another approach is to take observations in the submillimeter regime (e.g., Antarctic Submillimeter Telescope and Remote Observatory (AST/RO), JCMT, ASTE, Submillimeter Array (SMA), APEX, NANTEN2). Observations with high density or temperature tracers, such as higher transition lines of CO and its isotopes, are intensively done especially toward the central region of the galaxies. They are also capable of detecting individual star-forming regions selectively in the disk from the large-scale mapping of a galaxy (e.g., Muraoka et al. 2007), and the tight correlation of these dense gas and star-formation indicators in global analyses have been reported (Mauersberger et al. 1999, Komugi et al. 2007, Wilson et al. 2009). The detailed studies of the molecular clouds/clumps in the submillimeter regime provide us with the deeper knowledge of physical properties (Section 4), making it possible to search for precluster cores (e.g., Mizuno et al. 2010).

3. PHYSICAL PROPERTIES OF GIANT MOLECULAR CLOUDS

It is of great interest to investigate the physical properties of GMCs, which are important in the formation and evolution of GMCs, and to compare them among galaxies. It is common to use the 2.6 mm CO ($J = 1$–0) emission to trace molecular gas in galaxies. The intensity distribution of CO gives the size of a cloud, and a line profile gives the velocity dispersion of molecular gas. Comparisons of properties of GMCs are reviewed by Blitz et al. (2007), who used GMC catalogs from studies of nearby galaxies and a compilation of molecular clouds in the outer MW as observed by Dame, Hartmann & Thaddeus (2001) and cataloged in Rosolowsky & Leroy (2006), as well as Bolatto et al. (2008).

It is always difficult to make reliable comparisons of observed quantities taken by different instruments and observations. In order to ensure a reasonable and reliable comparison among different data sets, Rosolowsky & Leroy (2006) developed a sophisticated method, which takes into account the differences in resolutions and sensitivities of various observations. This method basically extrapolates the intensity distribution of a cloud to the zero level by using the intensity slope of the cloud that is truncated at the noise level. This method was used to derive cloud radius, line width, virial mass, and CO luminosity of GMCs (Blitz et al. 2007).

The X factor is the ratio of the H_2 molecular column density (per square centimeter) to the observed ^{12}CO integrated intensity (Kelvins kilometers per second). This is a useful factor, which conveniently relates the observed ^{12}CO intensity to the cloud mass. It has been an issue of broad and keen interest whether galaxies with varying metallicities have some common value X factor. A general method to derive the X factor is to compare the virial mass and the ^{12}CO ($J = 1$–0) luminosity of a cloud. In case the virial equilibrium holds in a cloud, the method gives a reliable conversion factor. If GMCs with a cloud radius, R, and mass, M, are self-gravitating, they obey the following relation:

$$M = R\sigma_v^2/(\mathrm{kG}), \tag{1}$$

where k is a constant of order unity, σ_v is the line width of the observed spectra, and G is the gravitational constant, respectively. If the column density of a GMC is uniform, M/R^2 is constant. Then we find that $\sigma_v \propto R^{0.5}$ and $M \propto \sigma_v^4$. GMCs in the MW are well relaxed gravitationally as argued in the ^{12}CO surveys of galactic molecular clouds (e.g., Solomon et al. 1987). Less massive clouds tend to show larger virial mass than the actual molecular mass, perhaps because they are too young to become fully relaxed by dissipating turbulent energy. Surveys of molecular clouds in ^{13}CO in the MW indicate that the degree of gravitational relaxation depends on $M(H_2)$ and

Figure 2

Plot of the virial mass of the giant molecular clouds as a function of CO luminosity [Large Magellanic Clouds (LMC), Fukui et al. 2008; Small Magellanic Clouds (SMC), Mizuno et al. 2001b; M31, Rolowsky 2007; M33, Engargiola et al. 2003; IC 10, Leroy et al. 2006; Milky Way, Dame et al. 2001].

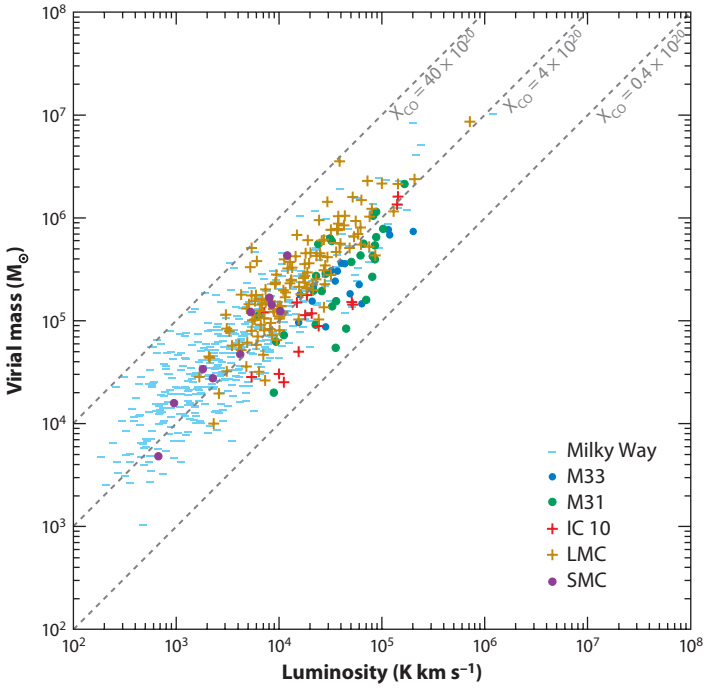

that ^{13}CO clouds of $M(H_2)$ greater than 10^4 $M_\odot$ have molecular mass consistent with the virial mass (Yonekura et al. 1997, Kawamura et al. 1998). A typical ratio of ^{12}CO to ^{13}CO cloud masses is ~3 (e.g., Mizuno et al. 1995), and the ^{13}CO cloud mass, 10^4 $M_\odot$, corresponds to $\sim 3 \times 10^4$ $M_\odot$ for a ^{12}CO cloud. GMCs with $M(H_2)$ greater than $\sim 10^5$ $M_\odot$ are likely gravitationally relaxed (Kawamura et al. 1998; Heyer, Carpenter & Snell 2001; Heyer et al. 2009). We use massive GMCs to derive the X factor in the followings and extrapolate the X factor to calculate the masses for less massive clouds having lower CO luminosities. A significant extended H_2 outer layer with no detectable CO is suggested in the N83 GMC in the SMC (Leroy et al. 2009a), but this seems to be an exceptional case with high UV flux and a low-metallicity environment.

We show a plot of the virial mass as a function of the CO luminosity in **Figure 2**. This plot is useful to derive the X factor, and the three lines of different values of the X factor are indicated by solid lines in **Figure 2**. **Table 2** lists the X factors derived for the individual galaxies. The scatter among these values is not so small, but **Figure 2** indicates that an X factor of 4.0×10^{20} cm^{-2} (K km s^{-1})$^{-1}$ is a reasonably good representation for these galaxies with a dispersion of $\sim 2.0 \times 10^{20}$ cm^{-2} (K km s^{-1})$^{-1}$. Among the five galaxies, points for the SMC having a low metallicity are located in the upper part, corresponding to the largest X factor higher than 10×10^{20} cm^{-2} (K km s^{-1})$^{-1}$. It is surprising that IC 10, which also has a low metallicity, is located relatively low, around 2.6×10^{20} cm^{-2} (K km s^{-1})$^{-1}$.

An independent method to derive the X factor is to make use of the gamma ray emission from a cloud. In interstellar space, there is a fairly uniform sea of cosmic ray protons that interact with interstellar low-energy hydrogen nuclei in clouds to create neutral pions. These pions quickly decay into two gamma rays. It is therefore possible to estimate the number of low-energy hydrogen nuclei in clouds from the gamma ray counts for an appropriate value of the cosmic-ray sea level. Such a gamma-ray based X factor is estimated to be 2.0×10^{20} cm^{-2} (K km s^{-1})$^{-1}$ for galactic clouds (Strong et al. 1988) and confirms that the virial method is a consistent way to estimate cloud mass.

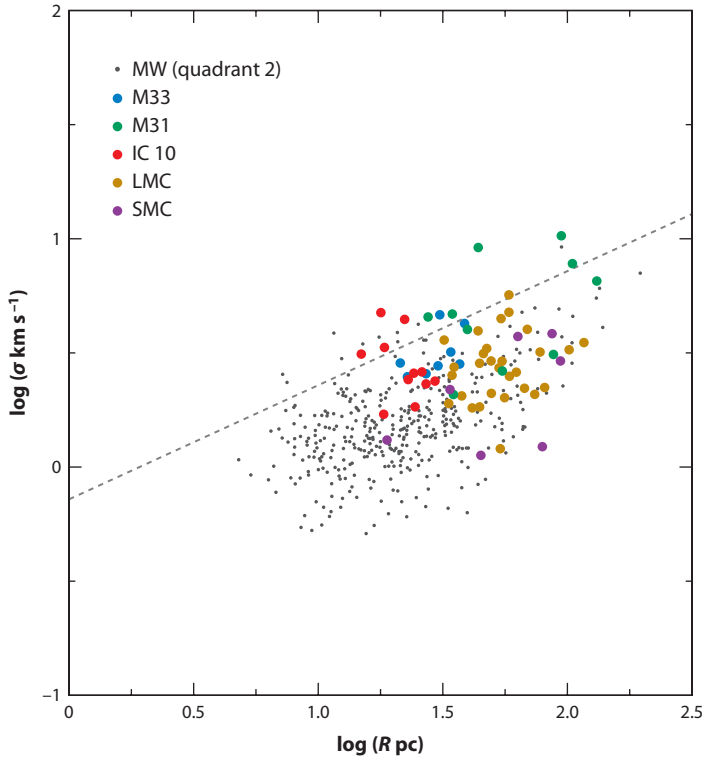

Figure 3

Line width–size relationship of the giant molecular clouds (GMCs). The dashed gray line is the relation found from the GMCs in the inner Milky Way (MW) (Solomon et al. 1987), showing some offset from the extragalactic GMCs [Large Magellanic Cloud (LMC), Fukui et al. 2008; Small Magellanic Cloud (SMC), Mizuno et al. 2001b; M31, Rosolowsky 2001; M33, Engargiola et al. 2003; IC 10, Leroy et al. 2006; MW, Dame et al. 2001].

Although gamma rays are not yet accurately measured outside the MW, this confirmation in the MW supports that the virial mass is applicable for extragalactic GMCs. We expect that gamma ray satellites including Fermi and Astrorivelatore Gamma Immagini Leggero may improve estimates on the X factor.

Some early studies used far-IR radiation to estimate cloud mass to derive an X factor (e.g., Israel 1997). It seems, however, difficult to use far-IR images to extract dust emission associated with a GMC (e.g., Bernard et al. 2008). Although the IR emission is correlated with GMCs to some extent, the correlation is not good enough to derive dust mass associated with a GMC. This is perhaps because the dust emission samples a much larger distance than the GMC size along a line of sight.

Figure 3 shows a plot of line width as a function of radius. This correlation has been studied in various samples of molecular clouds since the discovery of the relation by Larson (1981). The correlation between these quantities is not so high for extragalactic clouds. **Figure 3** shows that the line widths have a large scatter among galaxies as is most obvious when we compare IC 10 lying above the galactic line with the SMC in the bottom. The dynamic range may be too small to clearly see the trend. If we include the Galactic clouds a better hint of correlation is seen, which may be expressed as $\sigma_v \propto R^{0.5}$. Nevertheless, we note that there is a significant offset from the Galactic relation by Solomon et al. (1987). Blitz et al. (2007) argued that this may be due to the high values of T_A to define a cloud radius as done by Solomon et al. (1987) that may lead to an underestimate for a given line width. Bolatto et al. (2008) reanalyzed the Galactic data set considered under this argument and found that the Galactic molecular clouds are consistent with the extragalactic relations.

Figure 4 presents the mass distributions of five galaxies with power law; the spectral index is summarized in **Table 3**. These distributions are remarkably similar, in general, indicating that

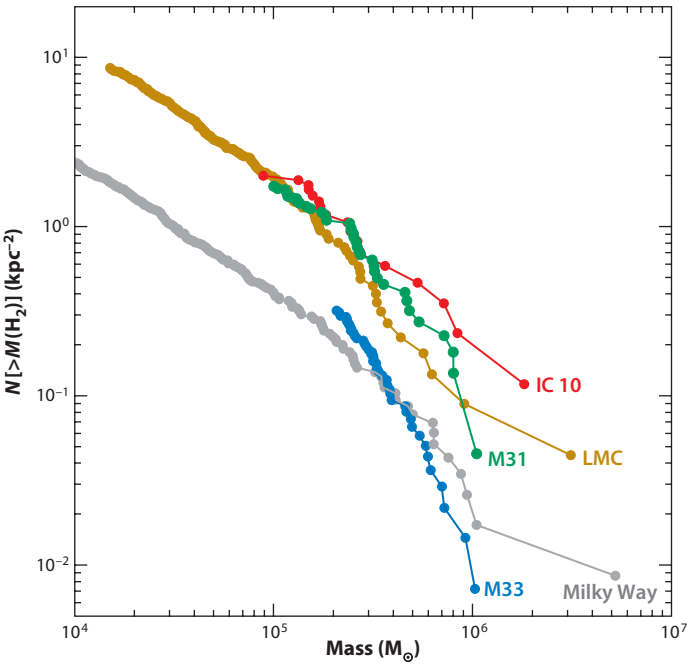

Figure 4

Cumulative mass distribution of the giant molecular clouds. The mass distributions have been normalized by the area surveyed in each [Large Magellanic Cloud (LMC), Fukui et al. 2008; M31, Rosolowsky 2007; M33, Engargiola et al. 2003; IC 10, Leroy et al. 2006; Milky Way, Dame et al. 2001].

the mass distributions are fairly common among most of the galaxies. M33 shows the steepest slope and may have a smaller mass of GMCs than the others. The alternative idea is that the mass spectrum becomes steeper in a high-mass range and that the high detection limit of the M33 survey of $\sim 10^5$ $M_\odot$ makes the difference. The steepness of the index of the mass spectrum in the high-mass range is also seen in the LMC survey (Kawamura et al. 2009; see also Rosolowsky 2005).

4. HIGH-MASS STAR FORMATION AND EVOLUTION OF GIANT MOLECULAR CLOUDS

4.1. Identification of High-Mass Star Formation

There has been an approach to study star-formation activities, the Kennicutt-Schmidt law, by using recent multiwavelength data sets for the star-formation indicators (Kennicutt 1989). At kiloparsec scales a strong correlation between the star-formation rate and molecular gas surface density is observed, and the star-formation rate has a steep dependence on total mass gas surface density, owing to the shallow radial profile of the atomic gas that dominates the total gas surface density

Table 3 Index of mass spectrum

Galaxy	Index	M_{min}^{a} x 10^5 ($M_\odot$)	Reference
LMC	−1.74 ± 0.08	0.5	Fukui et al. 2008
M31	−1.55 ± 0.20	1	Rosolowsky 2007
M33	−2.49 ± 0.48	1.5	Engargiola et al. 2003
IC 10	−1.71 ± 0.06	1	Leroy et al. 2006

[a]Minimum mass above which the index has been calculated.

for most radii. The relation is also observed where the atomic gas is dominant, suggesting that formation of molecular clouds is also an important factor of the star-formation rate (Paladino et al. 2006).

The evolution of GMCs substantially influences the evolution of galaxies. In particular, high-mass star formation in GMCs is a central event that affects galactic structure, energetics, and chemistry. A detailed understanding of high-mass star formation is therefore an important step for a better understanding of galaxy evolution. In Galactic molecular clouds, we are able to study the formation of stars from high to low mass including even brown dwarfs. In external galaxies, even those in the Local Group, such studies are limited to only the highest mass O stars as a result of limited sensitivity. Nevertheless it is worthwhile to learn how high-mass stars form in GMCs because high-mass stars impart the highest energies to the interstellar matter via UV photons, stellar winds, and supernova explosions. The most massive and most luminous O stars or their ionized regions are detectable uniformly over a single nearby galaxy. Only recently, unresolved distributions of stars with spectral types later than O are beginning to emerge from the *Spitzer* project, offering the potential to learn about the formation of less massive stars including B and A types (Whitney et al. 2008).

Young, high-mass stars are apparent at optical/radio wavelengths as the brightest members of stellar clusters or associations or by the Hα and radio continuum emission from HII regions. The positional coincidence between these signposts of high-mass star formation and GMCs is the most common method of identifying the star formation associated with individual clouds. Recently, new data sets in the IR wavelengths provide a large sample of high-mass star-forming regions (Calzetti et al. 2007). Such associations can be made with reasonable confidence when the source density is small enough that confusion is not important. When confusion becomes significant, however, conclusions can only be drawn by either making more careful comparisons at higher angular resolution or by adopting a statistical approach.

4.2. High-Mass Star Formation in the Large Magellanic Cloud

Figure 1 shows the molecular clouds detected with the NANTEN Survey on an optical image of the LMC. The 30 Dor region illustrates the most active site of high-mass star formation not only in the LMC but also in the Local Group. GMCs in the LMC appear to be spatially well separated, and it is possible to locate associated young objects with the GMCs. The complete sampling of the NANTEN survey allows us to make a statistical study of GMCs with various young objects including HII regions and young stellar clusters.

The most complete data sets of the young stars are available in the LMC. The data sets include catalogs of clusters and associations (e.g., Bica et al. 1996, 1999) and of optical and radio HII regions (Henize 1956; Davies, Elliott & Meaburn 1976; Kennicutt & Hodge 1986; Filipovic et al. 1996; Dickel et al. 2005). The colors of the stellar clusters are studied in detail at four optical wavelengths and are classified into an age sequence from SWB0 to SWB VII, where SWB0 is the youngest with an age of less than 10 Myr, SWB I is in a range of 10–30 Myr, and so on (Searle, Wilkinson & Bagnuolo 1980). Both data sets—of HII regions in Hα and of the radio thermal emission—can detect HII regions as faint as those equivalent to the ionization by an O5 star if a single ionizing source is assumed. We note that the detection limit of HII regions is quite deep, $L(\mathrm{H}\alpha) = 2 \times 10^{36}$ erg s^{-1}, corresponding to one-fourth the luminosity of the Orion Nebula.

Using the first NANTEN CO survey (Fukui et al. 1999, Mizuno et al. 2001c), the GMCs in the LMC were classified into three categories according to their associated young objects (Fukui et al. 1999, Yamaguchi et al. 2001a):

- Type I: Starless GMCs (no O stars); "starless" here indicates no associated O star capable of ionizing an HII region, which does not exclude the possibility of associated young stars later than B type.
- Type II: GMCs with HII regions only; those with small HII regions whose Hα luminosity is less than 10^{37} erg s^{-1}.
- Type III: GMCs with HII regions and stellar clusters; those with stellar clusters and large HII regions of Hα luminosity greater than 10^{37} erg s^{-1}.

Kawamura et al. (2009) used the second NANTEN catalog with improved detection limits to confirm this classification. For the updated sample of 272 GMCs in **Figure 1**, **Figure 5** shows the frequency distribution of the projected separation of young objects, that is, optical HII regions and stellar clusters (SWB 0 clusters) measured from the nearest significant CO-emitting GMC. Obviously, the youngest stellar clusters, SWB 0, and HII regions exhibit marked peaks within 50–100 pc, indicating their strong concentrations toward GMCs. Comparison of these distributions with a purely random distribution is shown by solid lines. The correlation with young clusters establishes the physical association with the GMCs. However, clusters older than SWB I show

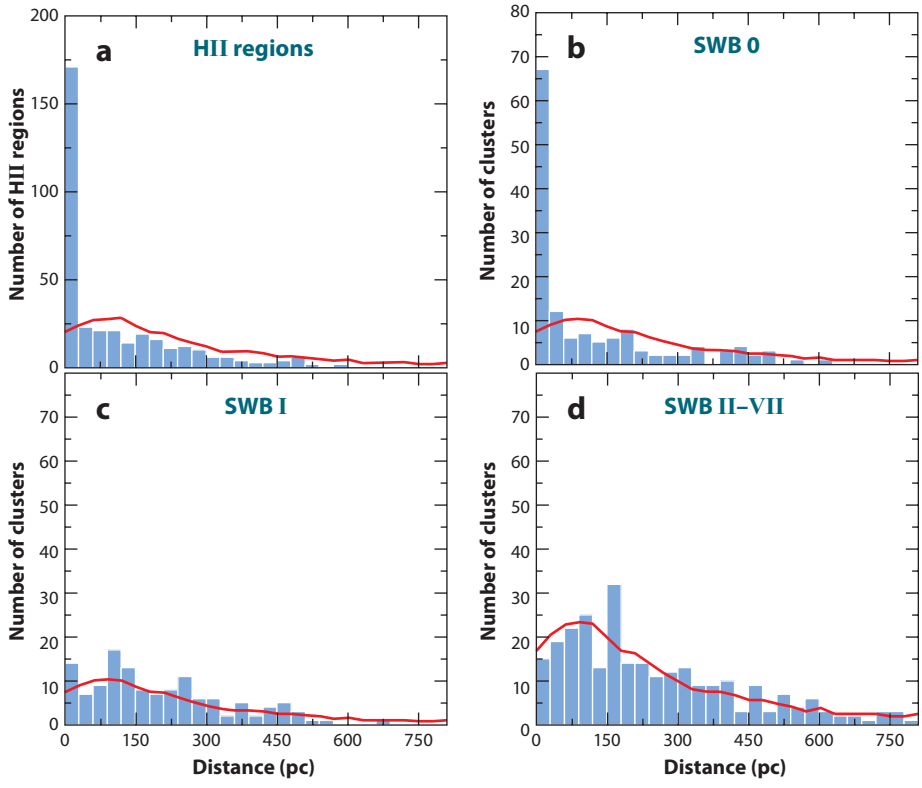

Figure 5

Frequency distribution of the projected distances of (*a*) the HII regions, (*b*) SWB 0 clusters (τ < 10 Myr), (*c*) SWB I clusters (10 Myr < τ < 30 Myr), and (*d*) SWB type II to VII clusters (30 Myr < τ; Bica et al. 1996) from the nearest molecular cloud in the Large Magellanic Clouds, respectively. Red lines show the frequency distribution of the distance when the HII regions and clusters are distributed randomly (Kawamura et al. 2009).

almost no correlation with GMCs, indicating that SWB I loses its memory for association with the natal GMC.

These GMC types may be interpreted as different generic types of GMCs. This is, however, not likely the case. A Type III GMC harbors stellar clusters with an age of 10 Myr, and this poses a lower limit for the age of GMCs to be 10 Myr. For a Type III GMC of typical mass, say $\sim 10^5$ $M_\odot$, the GMC cannot be formed in ~1 Myr, because the crossing timescale is estimated to be 10 Myr for a typical GMC of ~100-pc size and a typical HI line width of ~10 km s^{-1}. It is a reasonable assumption that the ~300 GMCs represent an evolutionary steady state because the three types are well mixed over the galaxy. This implies that the Type III GMC requires a precursor having a much lower star-formation activity of a 10-Myr timescale. These precursors are naturally represented by Type I/II GMCs.

The types are thus interpreted as an evolutionary sequence from Type I to III, and the lifetime of a GMC is estimated to be 20–30 Myr in total (Blitz et al. 2007, Kawamura et al. 2009). The stage after Type III is perhaps a very violent dissipation of GMCs due to UV photons, stellar winds, and supernova explosions from formed clusters as seen in 30 Dor in a most spectacular way. A summary of masses and sizes of GMCs are given for the three types in **Figure 6** (Kawamura et al. 2009).

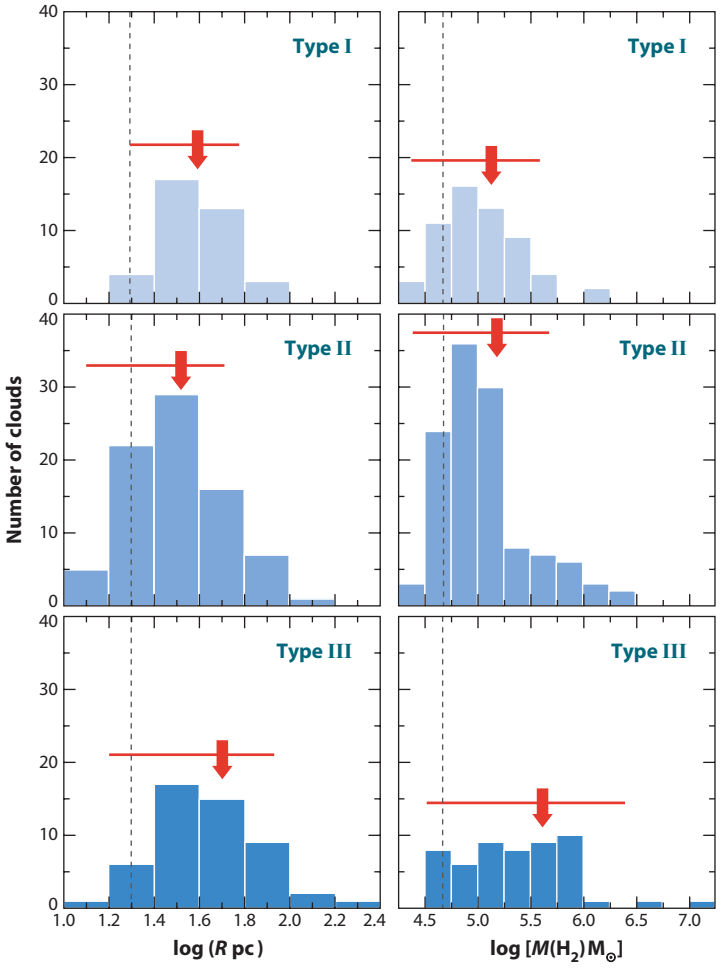

Figure 6

Histograms of radius R and mass $M(H_2)$ of the giant molecular clouds Type I, Type II, and Type III, respectively. Dashed gray lines indicate the completeness limit of the size (20 pc) and $M(H_2)$ (5×10^4 $M_\odot$). The red arrow and bar indicate the average and dispersion for each.

Table 4 Giant molecular cloud types and timescale in the Large Magellanic Cloud

Type	Number of clouds		Timescale (Myr)
	All clouds	GMCs	
I	72	46 (24%)	6
II	142	96 (50%)	13
III	58	49 (26%)	7
Total	272	191	26

Note: The second column presents the numbers and the ratios of the molecular clouds detected by the second NANTEN survey. The giant molecular clouds (GMCs) with mass above the completeness limit of the survey, 5×10^4 $M_\odot$, are shown in the third column and used to derive the timescale of each type. The formation of GMCs and clusters in the Large Magellanic Cloud (LMC) are assumed to be steady state, and each evolutionary timescale according to the above classification is estimated. First, the cloud dissipation timescale is estimated by using the age of the young clusters seen optically and the number of clusters associated with GMCs: ~66% of the youngest clusters of $\tau < 10$ Myr are associated with the GMCs. This result means the GMCs can survive during ~66% of the cluster age, 10 Myr, and are dissipated in a few million years after formation of clusters due to the UV photons from the clusters. The timescale for the GMC Type III is, thus, considered to be ~7 Myr. If massive star formation and cluster formation are assumed to occur at nearly steady state, the timescale for each stage is proportional to the number of the GMCs. Accordingly, the timescales for the GMCs Type I and II are estimated to be 6 Myr and 13 Myr, respectively.

Table 4 summarizes the results of the present comparison between GMCs and young objects. It shows that ~25% of the GMCs are starless in the sense that they are not associated with HII regions or young clusters. A comparison among the three Types indicates that the GMC size and mass tend to increase from Type I/II to Type III. Finally, **Figure 7** illustrates the interpretation that the three types represent an evolutionary trend of GMCs with probable timescales of each type derived from a steady state assumption.

4.3. High-Mass Star Formation in M33

None of the other galaxies in the present sample has such a complete record of interstellar gas and star formation as does the LMC. Owing to its proximity, large angular size, and rather low inclination, M33 is also a unique target and serves to derive additional indications about the high-mass star formation associated with GMCs. Engargiola et al. (2003) correlated the HII regions cataloged by Hodge et al. (1999) with the 149 GMCs in the M33 catalog. For reference, the completeness limit of the Hodge et al. (1999) catalog is $L(\mathrm{H}\alpha) = 3 \times 10^{35}$ erg s^{-1}; a similar range of HII regions is cataloged in the LMC and M33. Engargiola et al. (2003) assumed that an HII region is associated with a GMC if its boundary lies either within or tangent to a GMC. The result indicates that 36% of the flux from HII regions can be associated with the cataloged GMCs and suggests that more than 90% of the total flux of ionized gas from M33 originates from GMCs by correcting for the incompleteness of the GMCs. Within the uncertainties, essentially all of the flux from HII regions is consistent with an origin in GMCs.

Engargiola et al. (2003) counted the fraction of GMCs having at least one HII region. They defined the correlation length such that half the GMCs have at least one HII region within this distance. The correlation length for the GMCs and HII regions is 35 pc; a random distribution of GMCs and HII regions would return a correlation length of 80 pc. A study of each GMC and the distribution of HII regions show that as many as 100 GMCs (67%) are forming high-mass stars. They estimate that the number of totally obscured HII regions affects these results by at most 5%. The fraction of GMCs without star formation is estimated to be about one-third, a fraction similar to that in the LMC. The M33 study estimated the lifetime of GMCs to be ~20 Myr, also

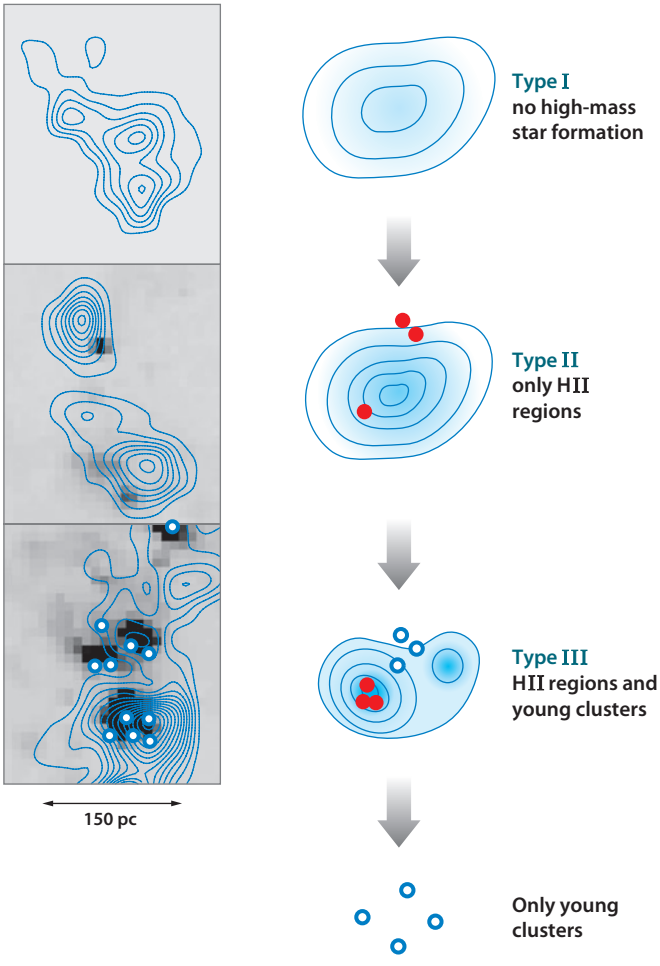

Figure 7

Evolutionary sequence of the molecular clouds. The left panels are examples of Large Magellanic Cloud (LMC) giant molecular cloud (GMC) Type I (GMC 225, LMC N J0547-7014 in Fukui et al. 2008), Type II (GMC 135, LMC N J0525-6609), and Type III (the northern part of GMC 197, LMC N J0540-7008) from the top panel, respectively. Each panel presents Hα images from Kim et al. (1999) with GMCs identified by CO contours obtained with NANTEN: The contour levels are from 1.2 K km s^{-1} with 1.2 K km s^{-1} intervals. Open blue circles indicate the position of young clusters (Bica et al. 1996). The right panels are cartoon illustrations for each evolutionary stage. Open blue circles and filled red circles represent young clusters and HII regions, respectively.

similar to that found for the LMC. The fraction of clouds without active star formation is much higher than that found in the vicinity of the Sun, where GMCs devoid of high-mass star formation are very rare within 2 kpc (Maddalena & Thaddeus 1985). It is unclear whether this difference is significant due to the small sample of the MW.

4.4. Individual High-Mass Star-Forming Regions

In the MW, most of the high-mass star formation occurs as OB associations like in Orion and η Car (e.g., Yonekura et al. 2005, Zinnecker & Yorke 2007 and references therein). In the present

sample of galaxies, there are a number of active star-formation regions including N159, N44 (Israel et al. 1996, Bolatto et al. 2000, Chen et al. 2009), N11 (Israel et al. 2003b) and R136 in 30 Dor in the LMC (Kutner et al. 1997; Johansson et al. 1998; Rubio, Paron & Dubner 2009), N66 in the SMC (Rubio et al. 2000), NGC604 in M33 (Tosaki et al. 2007a, Barbà et al. 2009), and Hubble V (e.g., Israel et al. 2003a). We shall look into some of these regions in order to have insights into details of high-mass star formation and molecular gas in connection with the evolution of GMCs.

The SEST 15-m millimeter telescope was used to map ^{12}CO [$J = 1$–0, 2–1, 3–2] transitions and ^{13}CO [$J = 1$–0 and 2–1] transitions in the LMC and SMC as ESO SEST's key project at resolutions around 10 pc in a series of papers starting from Israel et al. (1993). The observations are done mainly toward the molecular clouds associated with IR source, HII regions, and clusters, and the total coverage is about 2 and 1 square degrees in both the LMC and the SMC, each. These surveys identified some 50 molecular clumps/clouds of $\sim 10^4$ $M_\odot$, both isolated clumps and clumps embedded in GMCs, including the $J = 3$–2 image of 30 Dor; N159 W, E, and S in the LMC (Johansson et al. 1998); and N66, N88, and others in the SMC (Nikolic et al. 2007).

More extensive and accurate determinations of density and temperature are in progress at submillimeter wavelengths. The AST/RO 1.8-m telescope provided the first submillimeter view of dense clumps in the LMC that emit ^{12}CO ($J = 4$–3) emission (Bolatto, Israel & Martin 2005; Kim, Walsh & Xiao 2004). Pineda et al. (2008) used the NANTEN2 4-m telescope to observe the N159 GMC in several CO transitions (^{12}CO [$J = 1$–0, 3–2, 4–3 and $J = 7$–6], etc.) and derived that density toward the M159W is as high as 10^4 cm^{-3}. Minamidani et al. (2008) extended a ^{12}CO ($J = 3$–2) survey with ASTE to seven NANTEN GMCs and revealed that GMCs harbor ubiquitously dense molecular clumps, some of which are well correlated with star formation. Generally speaking, Type I GMCs have no such dense clumps and Type III GMCs have massive dense clumps. In star-forming regions the CO gas is warm with Tk $\sim$ 30–200 K, but in regions without star formation the CO gas is cool with Tk $\sim$ 10–30 K.

Most recently, Mizuno et al. (2010) analyzed submillimeter data (^{12}CO [$J = 1$–0, 3–2, 4–3 and upper limits for 7–6]: ^{13}CO [$J = 3$–2]) of three dense clumps in N159 named N159W, E, and S. **Figure 8*a*,*b*** show the distribution of ^{12}CO ($J = 3$–2) intensity, 24-μm sources, and the line intensity ratio of ^{12}CO ($J = 3$–2) and ^{12}CO ($J = 1$–0). Star formation is active in the north toward N159W and E as indicated by the associated mid-IR emission. The ^{12}CO ($J = 3$–2) and ($J = 1$–0) line intensity ratio is significantly enhanced toward N159W and E. They have densities of 3×10^3 cm^{-3} and temperatures of 70–80 K. The huge HII region N159 and numerous O stars are distributed mainly between the two clumps, where molecular gas appears depleted. However, N159S, which shows few signs of star formation, has a similar density of 1.6×10^3 cm^{-3} but has a significantly lower temperature of 30 K. This example illustrates that high-mass star formation causes strong dissipation of molecular gas and that active ongoing star formation occurs in dense clumps. A clump without star formation shows lower temperatures consistent with much less heating. A comparison between η Car in the MW and N159 indicates that the two regions are fairly similar to each other in terms of the number of high-mass stars and molecular mass. Another region of active star formation in the LMC is R136, which also exhibits violent dispersal of molecular gas under the effects of stellar winds and UV radiation. R136 is, perhaps, in a more advanced phase of cloud dispersal and much less molecular gas is observed (Fukui et al. 2008, Ott et al. 2008, Kawamura et al. 2009).

In M33, NGC 604 is the second luminous HII region in the Local Group and is a region of outstanding high-mass star formation (**Figure 1**). The GMA near NGC 604 was observed by a few groups (Wilson & Scoville 1990, Viallefond et al. 1992, Engargiola et al. 2003), and Wilson, Walker & Thornley (1997) observed two positions of the GMA in ^{12}CO [$J = 1$–0 and 3–2] and ^{13}CO ($J = 3$–2) lines. Tosaki et al. (2007a) used the 45-m and ASTE 10-m telescopes to observe

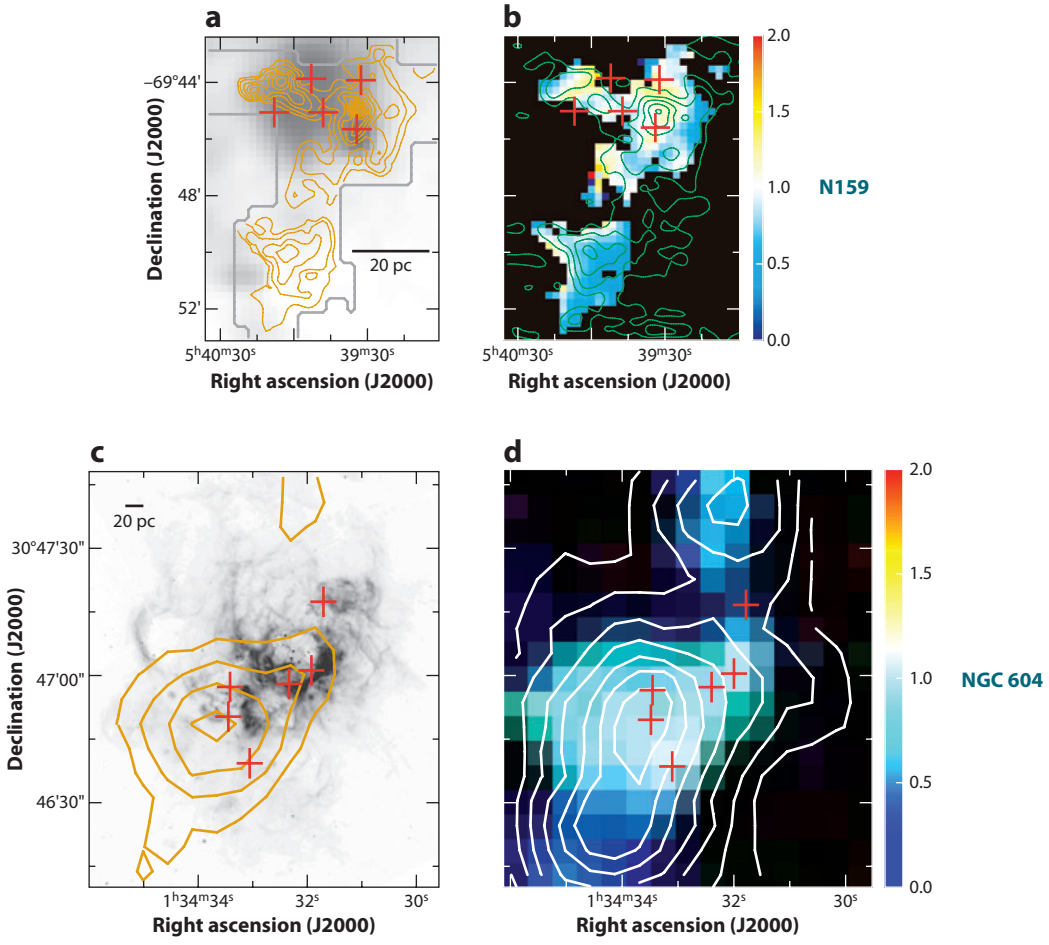

Figure 8

Active star-forming regions, N159 in the Large Magellanic Cloud (*a*, *b*) and NGC 604 in M33 (*c*,*d*). (*a*,*c*) Hα emission maps with ^{12}CO ($J = 3$–2) intensity in contours; (*b*,*d*) ^{12}CO ($J = 1$–0) intensity in contours superposed on the ratio maps of the intensities of ^{12}CO($J = 3$–2) and ^{12}CO ($J = 1$–0). The red crosses represent the positions of young clusters (*a*,*b*) and high-mass star formation (*c*,*d*), respectively (Tosaki et al. 2007a, Minamidani et al. 2008).

the ^{12}CO ($J = 1$–0 and $J = 3$–2) transitions. **Figure 8** shows the intensity ratio between $J = 3$–2 and $J = 1$–0 in the GMA, whose total mass is estimated to be $\sim 6 \times 10^5$ $M_\odot$. The average density of the GMA is $\sim 10^2$ cm^{-3}. The line ratio is enhanced along an arc-like shape in the south of NGC 604, and compact HII regions (Churchwell & Goss 1999) are distributed along the arc. The density and temperature of the arc are estimated to be 10^3–10^4 cm^{-3} and higher than 60 K. Tosaki et al. (2007a) suggest that second-generation star formation is occurring in the arc triggered by the first-generation star formation. This is another good example of strong gas dispersal by HII regions and the presence of warm and dense clumps in a GMC.

As suggested in NGC 604, triggering may be important in at least some of the star-forming regions. Supershells may play a role in such triggering as shown in the case of a supergiant shell, LMC4 (**Figure 9**) (Yamaguchi et al. 2001c). A comparison between supergiant shells and GMCs shows that at least about a third of the GMCs are located toward supershells

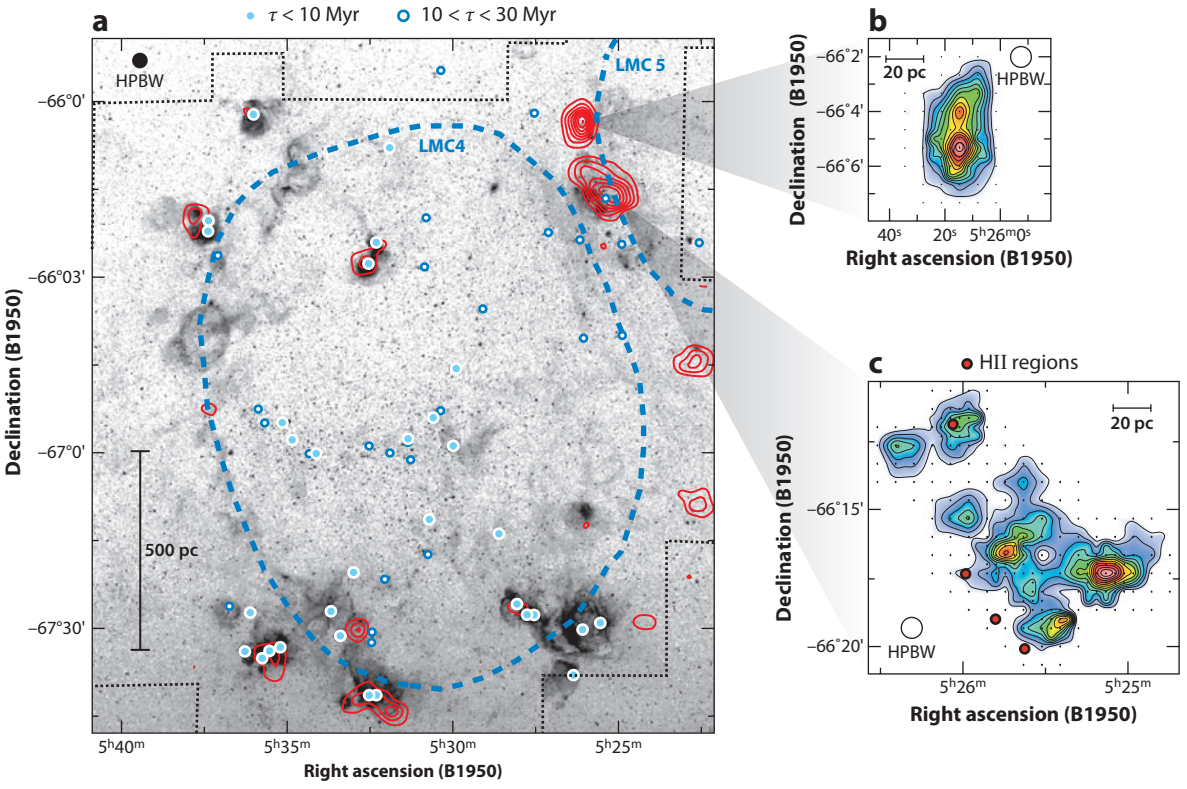

Figure 9

(*a*) CO ($J = 1$–0) emission of the Large Magellanic Cloud (LMC) obtained with NANTEN superposed on the Hα plate (Kennicutt & Hodge 1986). The red contours show velocity-integrated intensity of CO. The lowest contours and separation between contours are each 1 K km s^{-1}. The broken lines indicate the observed area. The boundary of the two supergiant shells, LMC4 and LMC5, is shown by the broken curved blue lines. The filled (*light blue*) and open (*dark blue*) circles are the clusters of $\tau < 10$ Myr and $10 < \tau < 30$ Myr (Bica et al. 1996), respectively. HPBW is a half power beam width. (*b*,*c*) CO ($J = 1$–0) intensity map obtained with the Swedish-ESO Submillimeter Telescope SEST. The lowest contours and separation between contours are each 2.5 K km s^{-1}. The dots on the map show the observed positions. The red circles indicate the position of the HII regions (Davies, Elliott & Meaburn 1976; Yamaguchi et al. 2001c).

(Yamaguchi et al. 2001b). Furthermore, such expanding shells may collide with each other, leading to enhanced triggered star formation. R136 is, for instance, located toward the overlapping area between two shells, LMC2 and 3, and may be the result of supersonic collisions between clouds. Triggered star formation is a long-standing subject and a number of numerical simulations have been made to date (e.g., Elmegreen & Lada 1977, Hosokawa & Inutsuka 2006). We suggest more elaborate theoretical studies of such triggering is desirable for a comparison with observations.

5. FORMATION OF GIANT MOLECULAR CLOUDS

5.1. Giant Molecular Clouds and Atomic Gas

It is a basic question how a GMC is formed via conversion of HI into H_2 and evolves to form stars and star clusters. Relevant theoretical processes of cloud formation are found in the extensive

review by McKee & Ostriker (2007). The importance of the ambient pressure and radiation field in the HI-H_2 conversion is suggested on scales of galaxies by theoretical studies (e.g., Elmegreen 1993). Observationally, it is crucial to identify atomic envelopes around GMCs and to make a detailed study of the distribution and kinematics of the envelope. In the MW, however, it is difficult to identify the HI gas associated with the GMCs because of the heavy crowding and contamination. A study of extragalactic resolved GMCs may offer a new and better insight into this issue. A few attempts were made to construct an empirical model of GMCs in dynamical equilibrium that consists of an atomic envelope and a molecular core and compared with observations of the active star-forming regions like the N159 region in the spectra of CO and H_2 (e.g., Pak et al. 1998). These studies indicate a possibility that GMCs may have large H_2 and HI envelopes with weak CO emission. The extensive samples of resolved GMCs in Section 3 may offer a good observational base to explore GMC formation further.

In the MW, Sato & Fukui (1978) and Hasegawa, Sato & Fukui (1983) identified cold HI gas associated with GMCs in M17 and W3/4 and suggested that the massive cold HI gas may be converted into molecular gas in these GMCs. Subsequently, Wannier, Lichten & Morris (1983) showed that five molecular clouds are associated with warm HI envelopes and suggested that such HI envelopes may be common among GMCs. Associations between GMCs and HI envelopes are, however, difficult to identify systematically and the available sample is restricted only to the solar vicinity (Andersson, Wannier & Morris 1991). As a result, the GMC-HI association has not been well established in the MW.

The extragalactic images of HI in **Figure 10** show that GMCs are located toward the peak of HI or HI filaments. Every GMC in each of the galaxies is found on a bright filament or clump of HI, but the reverse is not true: There are many bright filaments of HI without GMCs. In the LMC, GMCs are generally found at peaks of the HI but most of the short filaments have no associated CO. In the SMC, the HI is so widespread that the GMCs appear as small, isolated clouds in a vast sea of HI. In M33, the ratio of HI to CO in the filaments in the center of the galaxy is smaller than in the outer parts. Apparently, HI is a necessary but not a sufficient condition for the formation of GMCs in these galaxies. **Figure 10** shows that the GMCs form from the HI, rather than the HI being a dissociation product of GMCs as advocated before (e.g., Allen 2001). Most of the HI cannot be dissociated H_2 if the GMC lifetimes are as short as 20–30 Myr as cited in Section 4. It is reasonable that GMCs are forming in the HI filaments by thermal/gravitational instabilities and/or shock compressions, although the detailed processes of this conversion remain to be clarified. Because GMCs form from HI filaments, the HI filaments must form first as precursors to the GMCs.

The Magellanic system is an ideal laboratory to study GMC-HI association. Wong et al. (2009) made a comparative study of CO and HI on a global scale in the LMC by using the second NANTEN CO and ATCA HI data sets. These researchers used a 2D correlation between CO and HI as well as a two/one-Gaussian deconvolution of HI line profiles. They found in a more quantitative way than simple inspection that CO gas is associated with the HI gas with high intensity but that the intense HI is not always associated with CO. They also found that HI components with lower velocity dispersions show a weak trend of association with CO. This suggests that the energy dissipation of the HI gas may be connected to the GMC formation. For smaller scales of 10 pc in the N159 GMC region, Ott et al. (2008) presented evidence that this GMC is associated with localized intense HI gas by using the Mopra CO ($J = 1$–0) data. They tried some velocity-dependent analysis and noticed that the relatively bright peaks of the associated HI always show offsets in position from the peaks of GMCs. A larger sample of GMCs may shed more light on the GMC-HI correlation.

Figure 10

CO emission overlayed on maps of HI emission for (*a*) the Large Magellanic Cloud (Kim et al. 2003, Fukui et al. 2008) and (*b*) M33 (Deul & van der Hulst 1987, Engargiola et al. 2003).

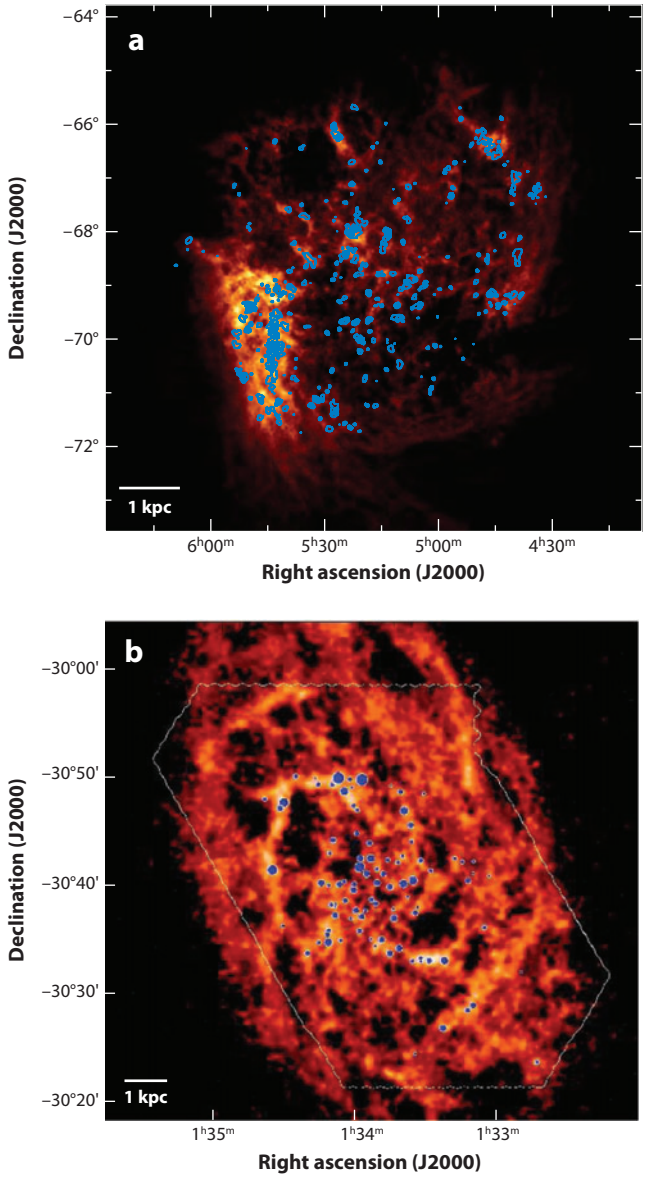

5.2. Three-Dimensional Correlation Method Between Giant Molecular Clouds and HI

Previous studies of star formation in galaxies employed 2D projection of HI intensity with large spatial averaging over ∼100 pc–1 kpc (e.g., Schmidt 1972, Kennicutt 1998). Typical CO and HI profiles indicate that the CO emission is highly localized in velocity; for instance, the HI emission ranges over 70 km s^{-1}, whereas the CO emission has a width less than 10 km s^{-1} in the LMC. The large velocity dispersion of HI is perhaps dominated by physically unrelated velocity components in the line of sight, and the HI gas associated with the CO gas may be only a small fraction of HI,

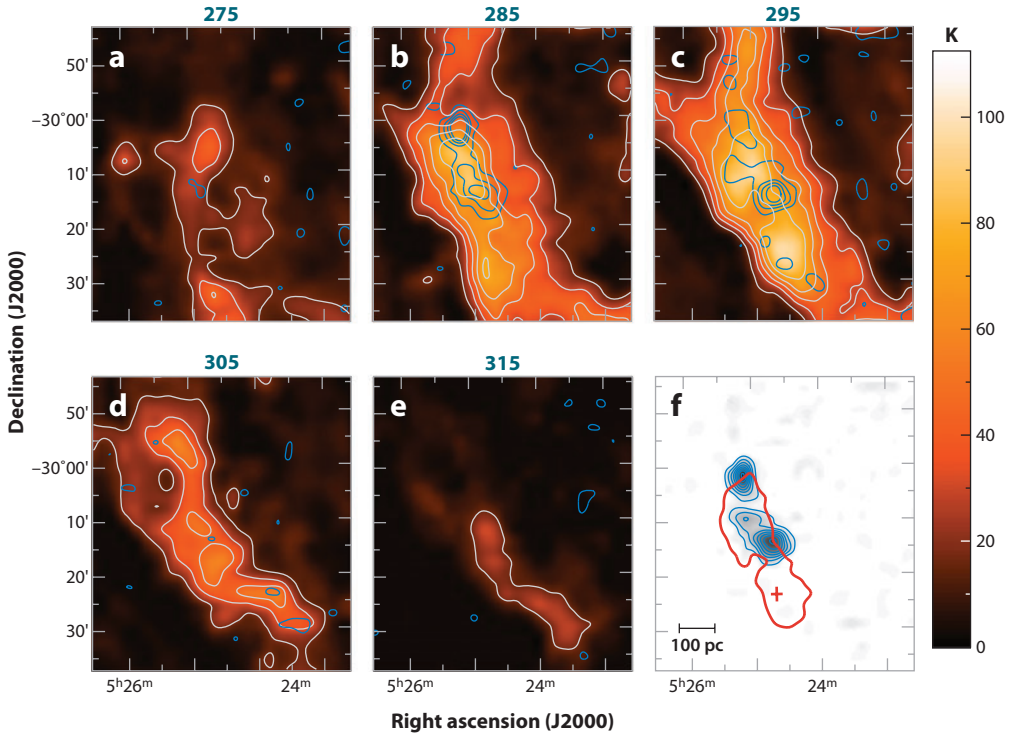

Figure 11

Velocity channel maps with a velocity interval of 10 km s^{-1} of the HI and CO emission of a Type II giant molecular cloud in the Large Magellanic Cloud. (*a–e*) The white contours show HI brightness temperature (Kim et al. 2003), and the blue contours show CO intensity (Fukui et al. 2008). HI contour levels are from 20 K with 20-K intervals, and CO contour levels are from 0.06 K with 0.12-K intervals. The central velocity of each panel is shown above each panel. (*f*) The total CO integrated intensity. The red contours and a red cross present the 80% level of the HI peak intensity and the position of the HI intensity peak, respectively (Fukui et al. 2009). CO contour levels are from 1.2 K km s^{-1} with 1.2 K km s^{-1} intervals. HI contour represents the 80% level of the HI peak intensity.

whose velocity is close to that of CO. Previous studies may therefore significantly overestimate the associated HI along the individual lines of sight.

Fukui et al. (2009) developed a 3D comparison of CO and HI in the LMC where the 3D data cube has a velocity axis in addition to two spatial axes projected on the sky; the 3D data cube of CO obtained with NANTEN (Fukui et al. 2008) and that of HI obtained with ATCA (Kim et al. 2003) consist of 1 million pixels having a size of 40 pc × 40 pc × 1.7 km s^{-1}. Fukui et al. (2009) chose 123 GMCs having simple single HI peaks from 272 GMCs for a detailed analysis. The average HI line widths, 14 km s^{-1}, are roughly three times larger than those of CO, 5 km s^{-1}, and the peak velocities of CO and HI show a good agreement within 2 km s^{-1}, supporting the association. Fukui et al. (2009) created velocity channel distributions of these GMCs and found that HI intensity integrated in the velocity range of CO shows well-defined association with CO. **Figure 11** shows an example of the velocity channel maps of the HI distribution associated with a Type II GMC. This GMC clearly shows the associated HI envelope. **Table 5** lists CO and HI parameters of the sample GMCs in the LMC. The CO distribution has small structures of ∼100 pc or less and the HI appears to be associated with the GMC at larger scales than the CO. They estimated the typical HI density to be ∼10 cm^{-3} by dividing the peak HI column density,

Table 5 Giant molecular cloud (GMC) types and parameters of the GMC and HI clouds in the Large Magellanic Cloud

GMC type	Number of GMCs	$M(H_2)$ ($\times 10^5$ $M_\odot$)	R (pc)	N(HI) ($\times 10^{21}$ cm^{-2})	ΔV(HI)[a] (km s^{-1})	ΔV(CO)[a] (km s^{-1})
Type I	72	2	37	...	...	5.0
Type II	142	2	33	...	...	4.8
Type III	58	5	51	...	...	6.9
	Selected[b]					
Type I	24	2	35	2.4	13.9	4.5
Type II	67	2	41	2.6	14.6	4.5
Type III	32	4	55	3.3	16.1	5.5

Note: Average properties of the GMCs (Fukui et al. 2009, Kawamura et al. 2009).
[a]Half-intensity full width derived by Gaussian fitting.
[b]Selected clouds having single-peaked HI profile.

2–5 $\times$ 10^{21} cm^{-2}, by the width of the HI envelope, 50–100 pc. As found by Ott et al. (2008) in N159, Fukui et al. (2009) noted that the HI peaks generally show offsets by 50–100 pc but lie well within 120 pc from GMC peaks, confirming the physical connection. This reveals that GMCs are associated with HI envelopes, whereas the HI envelopes are not always circularly symmetric, possibly affected by the elongation of the HI filament on a larger scale. They derived the average CO intensity I_{CO} (in Kelvins kilometers per second) by summing up the CO luminosity over all the pixels of a GMC and dividing it by the area of the GMC as measured in CO, and I_{HI} (in Kelvins kilometers per second) was calculated in the same manner. The regression between them is well fitted by a power law with an index of ~1.0, indicating a nearly linear correlation between I_{CO} and I_{HI} in a GMC. Fukui et al. (2009) provides first robust observational evidence for the warm HI envelope of a GMC.

5.3. HI Envelopes and the Giant Molecular Cloud Evolution

The HI envelope may indicate outer halos of GMCs as modeled by Pak et al. (1998). Fukui et al. (2009) found that the HI envelopes have a correlation with GMC types; the average HI intensities over the whole LMC are 34 ± 16 K(1σ), 47 ± 17 K, and 56 ± 19 K for Types I, II, and III, respectively, and that the HI intensity toward GMCs becomes larger with the activity of star formation. Fukui et al. (2009) argued that the GMC Type is also a sequence of mass and that Type III GMCs tends to be most massive among the three types. This led Fukui et al. (2009) to present a scenario that the enveloping HI gas may be accreting onto a GMC and that GMC mass increases in time. The accreted HI envelope is then converted into H_2 via reactions on grain surfaces owing to increased density and optical extinction in a timescale of 10 Myr (Spitzer 1978).

It could be discussed alternatively that HI gas may be supplied by recombination of HII into HI because Type II and Type III GMCs are associated with HII regions. This alternative, however, seems unlikely because the HII regions in Type II GMCs are all compact and are not a significant mass reservoir. It is also noted that the HI envelope in Type III GMCs is not matched spatially with the HII regions and clusters as seen in N159, for instance, where the HII regions and young clusters are confined into the north of the GMC and the HI is more widely distributed in the east and south (**Figure 7**). In the interpretation of Fukui et al. (2009), based on accretion, the HI line width may be dominated by infall motion of the HI envelope. This infall motion can arise mainly from gravity of a GMC and possibly from the converging flow driven by superbubbles.

For spherical accretion with a ∼40-pc radius of the HI gas having n(HI) ∼ 10 cm^{-3} at an infall speed of ∼7 km s^{-1}, half of the averaged HI line width, the mass accretion rate was estimated to be ∼0.05 $M_\odot$ year^{-1}. Over the typical timescale of the GMC evolution, ∼10 Myr, the increase in molecular mass amounts to ∼5 × 10^5 $M_\odot$ and is roughly consistent with the observed median value of the cloud mass ∼6 × 10^5 $M_\odot$ of a Type III GMC. This growth is perhaps terminated by the violent dispersal like that around R136.

Wong et al. (2009) showed that there are many places with high HI intensities without CO (see also Blitz et al. 2007). The HI gases showing the same intensity may actually be significantly different in density. As discussed by Wong et al. (2009), HI has two components, the hot tenuous one and the warm dense one. Because Fukui et al. (2009) eliminated the broader components by choosing relatively sharp single-peaked HI profiles, the analysis of Fukui et al. (2009) may focus only on the warm component, excluding the hot HI. We suggest that the high intensities without CO may represent the hot HI gas with lower density and higher temperature, which are not connected to GMC formation.

5.4. Formation of HI Filaments

Filamentary structures of HI are prominent in the present galaxies, and GMCs likely grow in these HI filaments (Section 5.3). It is therefore crucial to elucidate formation of the HI filaments of more than a few 100 pc in length. All the HI images of the galaxies in **Figure 10** are characterized by filamentary structures that often delineate holes in the atomic distribution (Oey 1996). In dwarfs, supershells may collect the atomic gas into such filamentary structures, whereas in spirals, density waves may play a major role in forming HI filaments in addition to supershells.

Yamaguchi et al. (2001b) made a systematic study of association between GMCs and supergiant shells in the LMC. They found that about one-third of GMCs, and accordingly their natal HI filaments, are associated with nine known supergiant shells. This suggests that shells play a role in formation of the HI filaments. Recent *Spitzer* images of the dust emission show a good correlation between HI shells and dust [Surveying the Agents of Galaxy Evolution (SAGE)] (Meixner et al. 2006). The *Spitzer* images illustrate that shell-like dust distributions are often surrounding evacuated regions without dust emission. This is a strong indication that these shell-like features are created by energetic events, as is most clearly illustrated in LMC4 and other prominent shells in the LMC (Meaburn 1980, Yamaguchi et al. 2001c, Book et al. 2009) and IC 10 (Wilcots & Miller, 1998). In IC 10, there is evidence that some of the holes are evacuated by the action of supernovae or stellar winds, which sweep up the atomic gas into the filamentary structure (Wilcots & Miller 1998). In contrast, most of the large holes observed in the M33 HI distribution are not likely to be caused by supernovae. The large holes require about 10^{53} erg to evacuate, but there are no obvious stellar clusters remaining at the center of the holes. Furthermore, X-ray emission is not concentrated in the holes. The large holes in M33 are thus likely to have a gravitational or density-wave origin. Small holes with D < 200 pc, on the other hand, are found to be well correlated with OB associations (Deul & van der Hulst 1987). Numerical simulations of the ISM in disk galaxies demonstrate that holes and filaments are the general outcome of stellar feedback in the multiphase interstellar matter (Wada & Norman 2001). Depending on how much gas is collected, and where in the gravitational potential of the galaxy the gas is located, a fraction of the atomic hydrogen is turned into molecular gas. But some other process, perhaps instabilities, also collects the gas into clouds. Yang et al. (2007) made an analysis of the Toomre Q factor in the LMC and showed that young stars and GMCs are preferentially located where the gas is gravitationally unstable.

5.5. Hydrostatic Pressure

In the case of the LMC, the intense HI gas is distributed to the east, where 30 Dor and the CO ridge are embedded, and this may suggest the tidal interaction plays a role in forming the kiloparsec-scale HI distribution in an interacting system (see Section 2.1.3.). More generally, Blitz & Rosolowsky (2006) developed an idea that the pressure in the galactic disk plays a macroscopic role in converting HI to H_2, though details of the microprocess of HI/H_2 conversion was left open. We note that photoionization, for instance, may play a role in such a microscopic process as discussed by Krumholz, McKee & Tumlinson (2008, 2009) and observationally tested by Leroy et al. (2009a). This pressure-dominated scenario seems to be promising to understand the large-scale background for conversion of HI into H_2 as demonstrated by a good correlation between the stellar mass density and the HI/H_2 gas ratio as a function of radius in spirals (Wong & Blitz 2002).

Blitz & Rosolowsky (2006) derived an expression of hydrostatic pressure as

$$P_{\rm hydro} = 0.84(G\Sigma_*)^{0.5}\ \Sigma_{\rm g} v_{\rm g}/(h_*)^{0.5}. \quad (2)$$

The quantities $v_{\rm g}$, the gas velocity dispersion, and h_*, the stellar scale-height, vary by less than a factor of two both within and among galaxies (van der Kruit & Searle 1981a,b; Kregel, van der Kruit & de Grijs 2002). The quantities Σ_*, the stellar surface density, and $\Sigma_{\rm g}$, the gas surface density, can be obtained from observations. Blitz & Rosolowsky (2004) showed that the location where the ratio of molecular to atomic gas is unity occurs at constant stellar surface density, suggesting that hydrostatic pressure is the key parameter governing the molecular gas fraction in galaxies. They found that the constancy holds to within 40% for 30 nearby galaxies. **Figure 12**, the results for 14 galaxies, shows that the galaxies all have similar almost linear slopes for the relationship $\sum_{H_2} / \sum_{HI} \propto P^{0.92}$, and all have the same constant of proportionality. The three exceptional galaxies, NGC 3627, NGC 4321, and NGC 4501, are interacting with their environments and

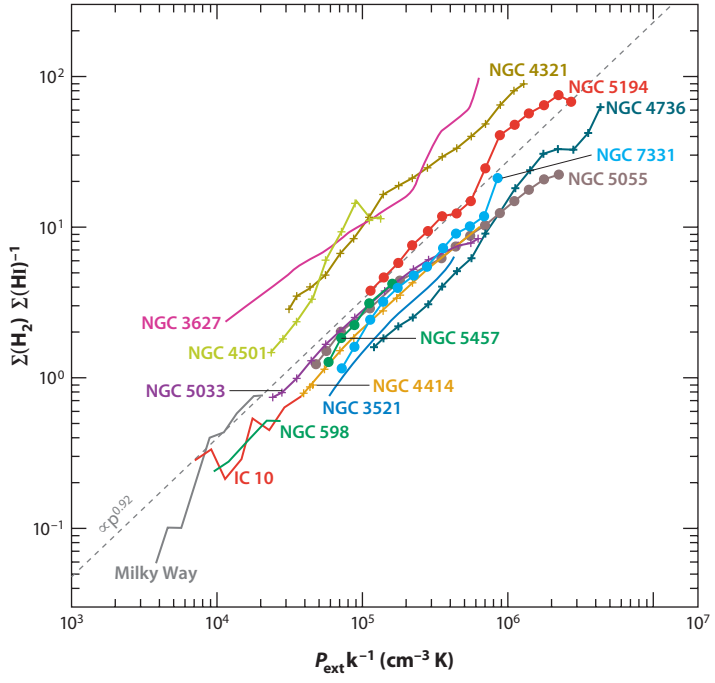

Figure 12

Plot of the ratio of molecular to atomic surface density as a function of hydrostatic pressure for 14 galaxies (Blitz & Rosolowsky 2006).

may be subject to additional pressure forces. Blitz & Rosolowsky expect that this relationship may hold at scales greater than the size of a typical GMC, ∼50 pc, where local pressure must be more important.

To summarize Section 5, on kiloparsec scales hydrostatic pressure offers a macroscopic condition that helps HI-H_2 conversion, whereas stellar feedback including supershells and/or density waves trigger formation of HI filaments on a few 100-pc scales. GMCs have HI envelopes and are perhaps formed by accreting HI gas by self-gravity in these HI filaments. The onset of the GMC formation may be explained by local dissipation of turbulent energy in the warm and dense HI gas.

6. CONCLUDING REMARKS

We have presented physical properties of resolved GMCs in some of the nearby Local Group galaxies, aiming at offering a template to extrapolate for understanding more distant galaxies. The GMCs share similar properties; the size of a GMC is 40–100 pc and the mass is 10^5–10^7 $M_\odot$. Virial method was applied to estimate mass and compared with L_{CO}, leading to an X factor of 4×10^{20} cm^{-2} (K km s^{-1})$^{-1}$, the CO-to-H_2 conversion factor, among six nearby galaxies harboring resolved GMCs. The conversion factor appears to vary from galaxy to galaxy, though metallicity may not be the only parameter that determines the factor. Their mass spectrum is steep, having a power-law index around ∼1.7.

For more distant galaxies only averaged properties are available. The surface mass density on kiloparsec scales generally ranges from 1–30 $M_\odot$ pc^{-2} in galactic disks. For the resolved GMCs surface molecular mass density is 10–100 $M_\odot$ pc^{-2} at a 50-pc scale, and that averaged at kiloparsecs is a few solar masses per square parsec. So, it seems the resolved GMC properties represent those with relatively lower molecular surface density. More studies must be conducted to understand detailed properties of GMCs in galaxies having higher molecular mass density with active star formation.

Star formation is linearly correlated with molecular mass on kiloparsec scales. The kiloparsec-scale averaged star formation is characterized by a uniform $L_{IR}/M(H_2)$ ratio around 10 $L_\odot$ $M_\odot{}^{-1}$. The scaling perhaps breaks at a length of less than 100 pc (Paladino et al. 2006), as is consistent with the GMC size of 100 pc. The resolved GMCs have revealed significant details of difference among GMCs in terms of high-mass star formation, as represented by the types. Resolved GMCs occur in three types according to the level of star-formation activity: Type I, Type II, and Type III. They probably represent an evolutionary sequence over a lifetime of 20–30 Myr.

A new 3D correlation study (Fukui et al. 2009) between GMCs and HI has revealed that GMCs are associated with HI envelopes. The HI envelopes may be in dynamical equilibrium or may be accreting onto GMCs to increase the mass via HI-H_2 conversion. Such a mass-wise growth mechanism is to be elaborated further theoretically, including the initial onset of accretion. GMCs are always located toward HI filaments. HI filaments, the birthplaces of GMCs, may be formed by supershells driven by energetic events or by density waves in spirals. On a global scale of kiloparsecs, hydrostatic pressure is also likely playing a role in forming HI filaments and therefore in initiating GMC formation.

Future higher resolution studies with ALMA will be able to resolve more than 1,000 galaxies at a resolution better than 40 pc. Such datasets will offer a remarkably detailed view of GMCs in galaxies and a deeper insight into the galactic evolution. It is particularly interesting to clarify whether the high molecular mass density in active galaxies is due to a higher number density of GMCs or due to intrinsic high mass of each GMC, that is, a more massive population of GMCs than discussed here. Further observations with recent IR satellites, such as *Herschel*, will reveal young objects with a lower mass or earlier evolutionary stage as well as cold dust and will make

it possible to study the ISM and star formation in various phases [e.g., Herschel Inventory of The Agents of Galaxy Evolution (HERITAGE) in the Magellanic Clouds and Herschel M33 extended survey (HERM33ES)]. HI images with the Square Kilometer Array are also important to correlate HI and CO in detail to explore HI-H_2 conversion, along with future powerful IR imaging instruments like the *Space Infrared Telescope for Cosmology and Astrophysics* telescope to sensitively probe star formation.

DISCLOSURE STATEMENT

The authors are not aware of any affiliations, memberships, funding, or financial holdings that might be perceived as affecting the objectivity of this review.

ACKNOWLEDGMENTS

We would like to express our gratitude to the editor, E. van Dishoeck, for her fruitful comments and discussion. We acknowledge all our coworkers who have provided their data as well as figures and are thankful to the expert readers: L. Blitz, A. Bolatto, K. Kohno, A. Leroy, T. Minamidani, A. Mizuno, N. Mizuno, T. Okuda, T. Onishi, E. Rosolowsky, M. Rubio, T. Tosaki, H. Yamamoto. In preparing this review, we made use of the search and archive facilities provided by NASA's Astrophysics Data System Bibliographic Service, NASA/IPAC Extragalactic Database, and SIMBAD Astronomical Database provided by CDS.

LITERATURE CITED

Allen RJ. 2001. *Gas and Galaxy Evolution*, *ASP Conf. Proc.*, Vol. 240, ed. JE Hibbard, M Rupen, JH van Gorkom, p. 331. San Francisco: Astron. Soc. Pac.
Andersson B-G, Wannier PG, Morris M. 1991. *Ap. J.* 366:464
Barbà RH, Maíz A, Jesús PE, Rubio M, Bolatto A, et al. 2009. *Ap. Space Sci.* 324:309
Bekki K, Chiba M. 2005. *MNRAS* 356:680
Bernard J-P, Reach WT, Paradis D, Meixner M, Paladini R, et al. 2008. *Astron. J.* 136:919
Bica E, Claria JJ, Dottori H, Santos JFC Jr, Piatti AE. 1996. *Ap. J. Suppl. Ser.* 102:57
Bica E, Dutra CM. 2000. *Astron. J.* 119:1214
Bica ELD, Schmitt HR. 1995. *Ap. J. Suppl. Ser.* 101:41
Bica ELD, Schmitt HR, Dutra CM, Oliveira HL. 1999. *Astron. J.* 117:238
Blitz L. 1993. *Protostars and Planets III*, ed. E Levy, JI Lunine, TM Bania, p. 125. Tucson: Univ. Ariz. Press
Blitz L, Fukui Y, Kawamura A, Leroy A, Mizuno N, Rosolowsky E. 2007. *Protostars and Planets V*, ed. B Reipurth, D Jewitt, K Keil, p. 81. Tucson: Univ. Ariz. Press, and Houston: Lunar and Planet. Inst.
Blitz L, Rosolowsky E. 2004. *Ap. J.* 612:L29
Blitz L, Rosolowsky E. 2006. *Ap. J.* 650:933
Blitz L, Thaddeus P. 1980. *Ap. J.* 241:676
Bolatto AD, Israel FP, Martin CL. 2005. *Ap. J.* 633:210
Bolatto AD, Jackson JM, Israel FP, Zhang X, Kim S. 2000. *Ap. J.* 545:234
Bolatto AD, Jackson JM, Wilson CD, Moriarty-Schieven G. 2000. *Ap. J.* 532:909
Bolatto AD, Leroy AK, Rosolowsky E, Walter F, Blitz L. 2008. *Ap. J.* 686:948
Bolatto AD, Simon JD, Stanimirović S, van Loon JTh, Shah RY, et al. 2007. *Ap. J.* 655:212
Book LG, Chu Y-H, Gruendl RA. 2008. *Ap. J. Suppl. Ser.* 175:165
Book LG, Chu Y-H, Gruendl RA, Fukui Y. 2009. *Astron. J.* 137:3599
Calzetti D, Kennicutt RC, Engelbracht CW, Leitherer C, Draine BT, et al. 2007. *Ap. J.* 666:870
Chen C-HR, Chu Y-H, Gruendl RA, Gordon KD, Heitsch F. 2009. *Ap. J.* 695:511
Churchwell E, Goss WM. 1999. *Ap. J.* 514:188

Cohen RS, Dame TM, Garay G, Montani J, Rubio M, Thaddeus P. 1988. *Ap. J.* 331:L95
Combes F. 1991. *Annu. Rev. Astron. Astrophys.* 29:195
Crosthwaite LP, Turner JL, Buchholz L, Ho PTP, Martin RN. 2002. *Astron. J.* 123:1892
Dame TM, Hartmann D, Thaddeus P. 2001. *Ap. J.* 547:792
Dame TM, Ungerechts H, Cohen RS, de Geus EJ, Grenier IA, et al. 1987. *Ap. J.* 322:706
Davies RD, Elliott KH, Meaburn J. 1976. *MmRAS* 81:89
Deul ER, van der Hulst JM. 1987. *Astron. Astrophys. Suppl. Ser.* 67:509
Dickel JR, McIntyre VJ, Gruendl RA, Milne DK. 2005. *Astron. J.* 129:790
Draine BT, Li A. 2007. *Ap. J.* 657:810
Dufour RJ. 1984. *Struct. Evol. Magellanic Clouds* 108:353
Elmegreen BG. 1989. *Ap. J.* 344:306
Elmegreen BG. 1993. *Ap. J.* 411:170
Elmegreen BG, Lada CJ. 1977. *Ap. J.* 214:725
Elmegreen BG, Morris M, Elmegreen DM. 1980. *Ap. J.* 240:455
Engargiola G, Plambeck RL, Rosolowsky E, Blitz L. 2003. *Ap. J. Suppl. Ser.* 149:343
Feast M. 1999. *New Views of the Magellanic Clouds*, *IAU Symp.* 190, ed. YH Chu, N Suntzeff, J Hesser, D Bohlender, p. 542. San Francisco: Astron. Soc. Pac.
Filipovic MD, White GL, Haynes RF, Jones PA, Meinert D, et al. 1996. *Astron. Astrophys. Suppl. Ser.* 120:77
Fujimoto M, Sofue Y. 1976. *Astron. Astrophys.* 47:263
Fukui Y, Kawamura A, Minamidani T, Mizuno Y, Kanai Y, et al. 2008. *Ap. J. Suppl. Ser.* 178:56
Fukui Y, Kawamura A, Wong T, Murai M, Iritani H, et al. 2009. *Ap. J.* 705:144
Fukui Y, Mizuno N, Yamaguchi R, Mizuno A, Onishi T, et al. 1999. *Publ. Astron. Soc. Jpn.* 51:745
Fukui Y, Mizuno N, Yamaguchi R, Mizuno A, Onishi T, et al. 2001. *Publ. Astron. Soc. Jpn.* 53:41
Gallagher JS III, Hunter DA, Gillett FC, Rice WL. 1991. *Ap. J.* 371:142
Gardiner LT, Noguchi M. 1996. *MNRAS* 278:191
Garnett DR. 1990. *Ap. J.* 363:142
Genzel R, Stutzki J. 1989. *Annu. Rev. Astron. Astrophys.* 27:41
Gordon KD, Clayton GC, Misselt KA, Landolt AU, Wolff MJ. 2003. *Ap. J.* 594:279
Gratier P, Braine J, Rodriguez-Fernandez NJ, Israel FP, Schuster KF, et al. 2010. *Astron. Astrophys.* 512:68
Harris J. 2007. *Ap. J.* 658:345
Hasegawa T, Sato F, Fukui Y. 1983. *Astron. J.* 88:658
Helfer TT, Thornley MD, Regan MW, Wong T, Sheth K, et al. 2003. *Ap. J. Suppl. Ser.* 145:259
Henize KG. 1956. *Ap. J. Suppl. Ser.* 2:315
Heyer MH, Carpenter JM, Snell RL. 2001. *Ap. J.* 551:852
Heyer MH, Corbelli E, Schneider SE, Young JS. 2004. *Ap. J.* 602:723
Heyer MH, Krwczyk C, Duval J, Jackson JM. 2009. *Ap. J.* 699:1092
Hilditch RW, Howarth ID, Harries TJ. 2005. *MNRAS* 357:304
Hodge P, Lee MG. 1990. *Publ. Astron. Soc. Pac.* 102:26
Hodge PW, Balsley J, Wyder TK, Skelton BP. 1999. *Publ. Astron. Soc. Pac.* 111:685
Hosokawa T, Inutsuka S-I. 2006. *Ap. J.* 646:240
Hubble EP. 1925. *Ap. J.* 62:409
Huchtmeier WK, Seiradakis JH, Materne J. 1981. *Astron. Astrophys.* 102:134
Indebetouw R, Whitney BA, Kawamura A, Onishi T, Meixner M, et al. 2008. *Astron. J.* 136:1442
Israel FP. 1997. *Astron. Astrophys.* 328:471
Israel FP, Baas F, Rudy RJ, Skillman ED, Woodward CE. 2003a. *Astron. Astrophys.* 397:87
Israel FP, Bontekoe TR, Kester DJM. 1996. *Astron. Astrophys.* 308:723
Israel FP, de Graauw Th, Johansson LEB, Booth RS, Boulanger F, et al. 2003b. *Astron. Astrophys.* 401:99
Israel FP, de Graauw Th, van de Stadt H, de Vries CP. 1986. *Ap. J.* 303:186
Israel FP, Johansson LEB, Lequeux J, Booth RS, Nyman LA, et al. 1993. *Astron. Astrophys.* 276:25
Israel FP, Johansson LEB, Rubio M, Garay G, de Graauw Th, et al. 2003c. *Astron. Astrophys.* 406:817
Israel FP, Maloney PR, Geis N, Herrmann F, Madden SC, et al. 1996. *Ap. J.* 465:738
Jarrett TH, Chester T, Cutri R, Schneider SE, Huchra JP. 2003. *Astron. J.* 125:525
Johansson LEB, Greve A, Booth RS, Boulanger F, Garay G, et al. 1998. *Astron. Astrophys.* 331:857

Kawamura A, Mizuno Y, Minamidani T, Filipovic MD, Staveley-Smith L, et al. 2009. *Ap. J. Suppl. Ser.* 184:1
Kawamura A, Onishi T, Yonekura Y, Dobashi K, Mizuno A, et al. 1998. *Ap. J. Suppl. Ser.* 117:387
Kennicutt RC Jr. 1989. *Ap. J.* 344:685
Kennicutt RC Jr. 1998. *Ap. J.* 498:541
Kennicutt RC Jr, Hodge PW. 1986. *Ap. J.* 306:130
Kim S, Dopita MA, Staveley-Smith L, Bessel MS. 1999. *Astron. J.* 118:2797
Kim S, Staveley-Smith L, Dopita MA, Sault RJ, Freeman KC, et al. 2003. *Ap. J. Suppl. Ser.* 148:473
Kim S, Walsh W, Xiao K. 2004. *Ap. J.* 616:865
Kobulnicky HA, Skillman ED. 1997. *Ap. J.* 489:636
Koda J, Scoville N, Sawada T, La Vigne MA, Vogel SN, et al. 2009. *Ap. J.* 700:L132
Kohno K, Nakanishi K, Tosaki T, Muraoka K, Miura R, et al. 2008. *Ap. Space Sci.* 313:279
Komugi S, Kohno K, Tosaki T, Nakanishi H, Onodera S, et al. 2007. *Publ. Astron. Soc. Jpn.* 59:55
Kregel M, van der Kruit PC, de Grijs R. 2002. *MNRAS* 334:646
Krumholz MR, McKee CF, Tumlinson J. 2008. *Astron. Astrophys.* 689:865
Krumholz MR, McKee CF, Tumlinson J. 2009. *Astron. Astrophys.* 693:216
Kuno N, Sato N, Nakanishi H, Hirota A, Tosaki T, et al. 2007. *Publ. Astron. Soc. Jpn.* 59:117
Kutner ML, Rubio M, Booth RS, Boulanger F, de Graauw Th, et al. 1997. *Astron. Astrophys. Suppl. Ser.* 122:255
Larson RB. 1981. *MNRAS* 194:809
Leroy A, Bolatto A, Walter F, Blitz L. 2006. *Ap. J.* 643:825
Leroy AK, Bolatto A, Bot C, Engelbracht CW, Gordon K, et al. 2009a. *Ap. J.* 702:352
Leroy AK, Walter F, Bigiel F, Usero A, Weiss A, et al. 2009b. *Astron. J.* 137:4670
Loinard L, Dame TM, Heyer MH, Lequeux J, Thaddeus P. 1999. *Astron. Astrophys.* 351:1087
Maddalena RJ, Thaddeus P. 1985. *Ap. J.* 294:231
Massey P, Armandroff TE. 1995. *Astron. J.* 109:2470
Massey P, Hodge PW, Holmes S, Jacoby G, King NL, et al. 2001. *Bull. Am. Astron. Soc.* 33:1496
Mateo ML. 1998. *Annu. Rev. Astron. Astrophys.* 36:435
Mauersberger R, Henkel C, Walsh W, Schulz A. 1999. *Astron. Astrophys.* 341:256
McAlary CW, Madore BF, McGonegal R, McLaren RA, Welch DL. 1983. *Ap. J.* 273:539
McKee C, Ostriker EC. 2007. *Annu. Rev. Astron. Astrophys.* 45:565
Meaburn J. 1980. *MNRAS* 192:365
Meixner M, Gordon KD, Indebetouw R, Hora JL, Whitney B, et al. 2006. *Astron. J.* 132:2268
Minamidani T, Mizuno N, Mizuno Y, Kawamura A, Onishi T, et al. 2008. *Ap. J. Suppl. Ser.* 175:485
Mizuno A, Onishi T, Yonekura Y, Nagahama T, Ogawa H, Fukui Y. 1995. *Ap. J.* 445:L161
Mizuno A, Yamaguchi R, Tachihara K, Toyoda S, Aoyama H, et al. 2001a. *Publ. Astron. Soc. Jpn.* 53:1071
Mizuno N, Muller E, Maeda H, Kawamura A, Minamidani T, et al. 2006. *Ap. J.* 643:L107
Mizuno N, Rubio M'onica, Mizuno A, Yamaguchi R, Onishi T, Fukui Y. 2001b. *Publ. Astron. Soc. Jpn.* 53:L45
Mizuno N, Yamaguchi R, Mizuno A, Rubio M, Abe R, et al. 2001c. *Publ. Astron. Soc. Jpn.* 53:971
Mizuno Y, Kawamura A, Onishi T, Minamidani T, Muller E, et al. 2010. *Publ. Astron. Soc. Jpn.* 62:51
Muller E, Stanimirovic S, Rosolowsky E, Staveley-Smith L. 2004. *Ap. J.* 616:845
Muller E, Staveley-Smith L, Zealey WJ. 2003. *MNRAS* 338:609
Murai T, Fujimoto M. 1980. *Publ. Astron. Soc. Jpn.* 32:581
Muraoka K, Kohno K, Tosaki T, Kuno N, Nakanishi K, et al. 2007. *Publ. Astron. Soc. Jpn.* 59:43
Nieten C, Neininger N, Guin M, Ungerechts H, Lucas R, et al. 2006. *Astron. Astrophys.* 453:459
Nikolic S, Garay G, Rubio M, Johannson LEB. 2007. Presented at Molecules in Space and Laboratory, Paris, Fr., May 14–18, p. 30
Oey MS. 1996. *Ap. J.* 467:666
Ohta K, Sasaki M, Saito M. 1988. *Publ. Astron. Soc. Jpn.* 40:653
Ohta K, Sasaki M, Yamada T, Saito M, Nakai N. 1992. *Publ. Astron. Soc. Jpn.* 44:585
Ohta K, Tomita A, Saito M, Sasaki M, Nakai N. 1993. *Publ. Astron. Soc. Jpn.* 45:L21
Ott J, Wong T, Pineda JL, Hughes A, Muller E, et al. 2008. *Publ. Astron. Soc. Aust.* 25:129
Pak S, Jaffe DT, van Dishoeck EF, Johansson LEB, Booth RS. 1998. *Ap. J.* 498:735
Paladino R, Murgia M, Helfer TT, Wong T, Ekers R, et al. 2006. *Astron. Astrophys.* 456:847
Pineda JL, Mizuno N, Stutzki J, Cubick M, Aravena M, et al. 2008. *Astron. Astrophys.* 482:197

Pineda JL, Ott J, Klein U, Wong T, Muller E, Hughes A. 2009. *Ap. J.* 703:736
Putman ME, Gibson BK, Staveley-Smith L, Banks G, Barnes DG, et al. 1998. *Nature* 394:752
Regan MW, Vogel SN. 1994. *Ap. J.* 434:536
Rolleston WRJ, Brown PJF, Dufton PL, Howarth ID. 1996. *Astron. Astrophys.* 315:95
Rolleston WRJ, Dufton PL, Fitzsimmons A, Howarth ID, Irwin MJ. 1993. *Astron. Astrophys.* 277:10
Rolleston WRJ, Dufton PL, McErlean ND, Venn KA. 1999. *Astron. Astrophys.* 348:728
Rosolowsky E. 2005. *Publ. Astron. Soc. Pac.* 117:1403
Rosolowsky E. 2007. *Ap. J.* 654:240
Rosolowsky E, Engargiola G, Plambeck R, Blitz L. 2003. *Ap. J.* 599:258
Rosolowsky E, Leroy A. 2006. *Publ. Astron. Soc. Pac.* 118:590
Rosolowsky E, Keto E, Matsushita S, Willner SP. 2007. *Ap. J.* 661:830
Rowan-Robinson M, Phillips TG, White G. 1980. *Astron. Astrophys.* 82:381
Rubio M, Contursi A, Lequeux J, Probst R, Barbà R, et al. 2000. *Astron. Astrophys.* 359:1139
Rubio M, Garay G, Montani J, Thaddeus P. 1991. *Ap. J.* 368:173
Rubio M, Lequeux J, Boulanger F. 1993. *Astron. Astrophys.* 271:9
Rubio M, Lequeux J, Boulanger F, Booth RS, Garay G, et al. 1996. *Astron. Astrophys. Suppl. Ser.* 118:263
Rubio M, Paron S, Dubner G. 2009. *Astron. Astrophys.* 505:177
Russell SC, Dopita MA. 1992. *Ap. J.* 384:508
Růžička A, Theis C, Palouš J. 2009. *Ap. J.* 691:1807
Sakamoto K, Ho PTP, Iono D, Keto ER, Mao R-Q, et al. 2006. *Ap. J.* 636:685
Sato F, Fukui Y. 1978. *Astron. J.* 83:1607
Schmidt Th. 1972. *Astron. Astrophys.* 16:95
Schuster KF, Kramer C, Hitschfeld M, Garcia-Burillo S, Mookerjea B. 2007. *Astron. Astrophys.* 461:143
Searle L, Wilkinson A, Bagnuolo WG. 1980. *Ap. J.* 239:803
Sheth K, Vogel SN, Wilson CD, Dame TM. 2008. *Ap. J.* 675:330
Skillman ED, Terlevich R, Melnick J. 1989. *MNRAS* 240:563
Solomon PM, Rivolo AR, Barrett J, Yahil A. 1987. *Ap. J.* 319:730
Sorai K, Hasegawa T, Booth RS, Rubio M, Morino J-I, et al. 2001. *Ap. J.* 551:794
Spitzer L. 1978. *Physical Processes in the Interstellar Medium*. New York: Wiley-Interscience. 333 pp.
Staveley-Smith L, Kim S, Putman M, Stanimirović S. 1998. *Rev. Mod. Astron.* 11:117
Strong AW, Bloemen JBGM, Dame TM, Grenier IA, Hermsen W, et al. 1988. *Astron. Astrophys.* 207:1
Thronson HA Jr, Hunter DA, Casey S, Harper DA. 1990. *Ap. J.* 355:94
Tosaki T, Miura R, Sawada T, Kuno N, Nakanishi K, et al. 2007a. *Ap. J.* 664:L27
Tosaki T, Shioya Y, Kuno N, Hasegawa T, Nakanishi K, et al. 2007b. *Publ. Astron. Soc. Jpn.* 59:33
van der Kruit PC, Searle L. 1981a. *Astron. Astrophys.* 95:105
van der Kruit PC, Searle L. 1981b. *Astron. Astrophys.* 95:116
van der Marel RP, Cioni M-RL. 2001. *Astron. J.* 122:1807
Viallefond F, Boulanger F, Cox P, Lequeux J, Perault M, Vogel SN. 1992. *Astron. Astrophys.* 265:437
Wada K, Norman CA. 2001. *Ap. J.* 547:172
Wannier PG, Lichten SM, Morris M. 1983. *Ap. J.* 268:727
Westerlund BE. 1997. *The Magellanic Clouds, Cambridge Astrophys. Ser., 29*. Cambridge, United Kingdom: Cambridge Univ. Press. 279 pp.
Whitney BA, Sewilo M, Indebetouw R, Robitaille TP, Meixner M, et al. 2008. *Astron. J.* 136:18
Wilcots EM, Miller BW. 1998. *Astron. J.* 116:2363
Wilson CD. 1992. *Ap. J.* 391:144
Wilson CD. 1995. *Ap. J.* 448:L97
Wilson CD, Reid IN. 1991. *Ap. J.* 366:L11
Wilson CD, Scoville N. 1990. *Ap. J.* 363:435
Wilson CD, Walker CE, Thornley MD. 1997. *Ap. J.* 483:210
Wilson CD, Warren BE, Israel FP, Serjeant S, Bendo G, et al. 2009. *Ap. J.* 693:1736
Wong T, Blitz L. 2002. *Ap. J.* 569:157
Wong T, Hughes A, Fukui Y, Kawamura A, Mizuno N, et al. 2009. *Ap. J.* 696:370
Yamaguchi R, Mizuno N, Mizuno A, Rubio M, Abe R, et al. 2001a. *Publ. Astron. Soc. Jpn.* 53:985

Yamaguchi R, Mizuno N, Onishi T, Mizuno A, Fukui Y. 2001b. *Publ. Astron. Soc. Jpn.* 53:959
Yamaguchi R, Mizuno N, Onishi T, Mizuno A, Fukui Y. 2001c. *Ap. J.* 553:L185
Yang C-C, Gruendl RA, Chu Y-H, Mac Low M-M, Fukui Y. 2007. *Ap. J.* 671:374
Yang H, Skillman ED. 1993. *Astron. J.* 106:1448
Yonekura Y, Asayama S, Kimura K, Ogawa H, Kanai Y, et al. 2005. *Ap. J.* 634:476
Yonekura Y, Dobashi K, Mizuno A, Ogawa H, Fukui Y. 1997. *Ap. J. Suppl. Ser.* 110:21
Yoshizawa AM, Noguchi M. 2003. *MNRAS* 339:1135
Young JS, Scoville NZ. 1991. *Annu. Rev. Astron. Astrophys.* 29:581
Young LM. 2001. *Astron. J.* 122:1747
Zaritsky D, Harris J, Thompson IB, Grebel EK. 2004. *Astron. J.* 128:1606
Zinnecker H, Yorke HW. 2007. *Annu. Rev. Astron. Astrophys.* 45:481

Annual Review of Astronomy and Astrophysics

Volume 48, 2010

Contents

Indexes

Errata

An online log of corrections to *Annual Review of Astronomy and Astrophysics* articles may be found at http://astro.annualreviews.org/errata.shtml